CHAPTER 3

RESULTS AND DISCUSSION

In these research project, three interesting studies have been proposed to achieve greener analytical methods for analyzing real samples. Initially, a simple and cost effective FIA manifold with spectrophotometric detector was describes for Ni(II) determination in waters using nitroso-R salt as complexing agent. Secondly a modified mini-CNC machine coupled with diode laser to obtain a new machine for fabrication of PMMA chips and used as micro reactor in the μFA manifold. Evaluation and characterization of the fabricated chips were also performed. Finally, a μFA manifold using the fabricated micro reactor with spectrophotometric detector was developed and tested for Zn(II) determination in waters. The detail studies will be discussed fully as follows:

3.1 Determination of Ni(II) by flow injection analysis

The flow injection system was used as a basis for development of a simple, rapid and reproducible method with low reagent consumption (comparison with the bath-wise method) for analysis of trace nickel. Appropriate flow injection conditions for analysis of nickel were achieved. The method is based on the measurement of absorbance rising from Ni(II)-nitroso-R complex in an ammonium acetate buffer solution, formed by the reaction between Ni(II) and nitroso-R salt.

3.1.1 Preliminary studied and selection of the absorption wavelength

The absorption spectra of Ni(II)- nitroso-R salt complex was recorded over a range from 380-700 nm against their nitroso-R salt blank, using JENWAY 6400

ลิขสิทธิ์มหาวิทยาลัยเชียงใหม่
Copyright© by Chiang Mai University
All rights reserved

spectrophotometer in conjunction with Jenway scan software connected to a PC as shown in Figure 3.1. In the aqueous medium, investigation was carried out to study the λ_{max} of Ni(II) under the given conditions; 2 and 3 mg L^{-1} of each studied Ni(II) ions solution mixed with 2.0 x 10^{-4} mole L^{-1} nitroso-R salt in sample cell. It was found that the significant overlapping of the absorption spectrum, the optimum conditions of complex products were studied at 490 nm, where the nitroso-R salt absorption was virtually absent. Therefore, the absorption wavelength of 490 nm was chosen as the optimum wavelength and used for subsequent experiments.

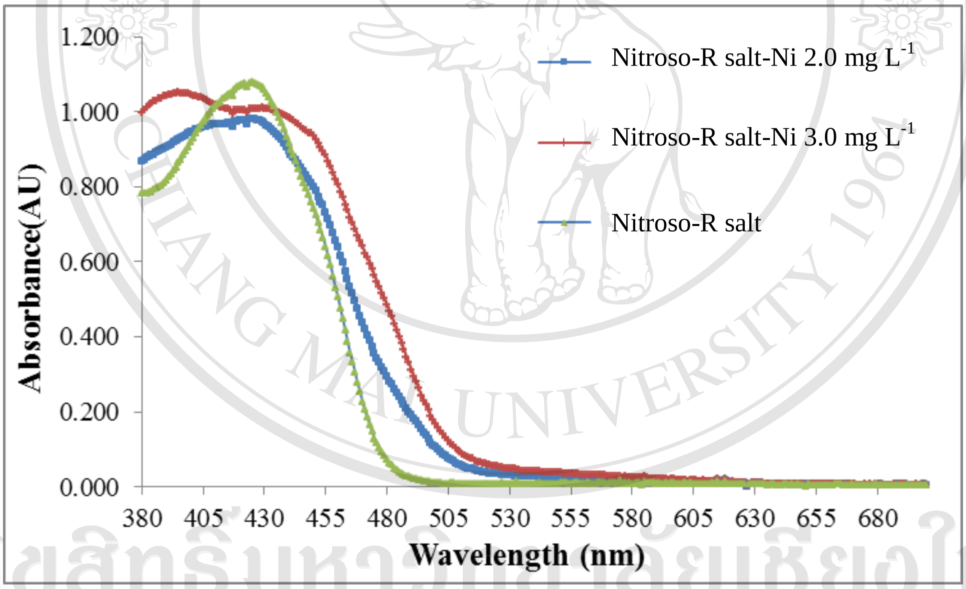

Figure 3.1 The absorbance of Ni(II)-nitroso-R salt complexes measured at various wavelength in the range from 380 to 700 nm with nitroso-R salt at pH 8.0; 2.0 × 10^{-4} mole L^{-1} nitroso-R salt

ลิขสิทธิ์มหาวิทยาลัยเชียงใหม่
Copyright© by Chiang Mai University
All rights reserved

3.1.2 The composition of Ni(II)-nitroso-R salt complex by mole-ratio method

The complex composition of Ni(II)-nitroso-R salt was studied by the mole-ratio method. This method, a series of complexes are prepared containing a fixed amount of Ni(II) ion, with a changing concentration of nitroso-R salt. The absorbances of these products are then measured with spectrometer (Jenway 6400). A resulting plot of absorbance vs. ligand-to-metal ratio initially increases and then develops constant one the ligand to metal ratio has been accomplished. The point at which the slope of the line changes relates to the nitroso-R: nickel ratio of the complex. The mole-ratio methods of Ni(II)-nitroso-R salt complex was definite as a series of solution were prepared in which Ni concentrations were fixed whereas the nitroso-R salt concentration was varied.

The numerous concentrations of nitroso-R salt (0-6 x 10^{-5} mol L^{-1}) were added to solution containing 1.0×10^{-5} mol L^{-1} of Ni, 5 mL of 0.5 mol L^{-1} of ammonium acetate buffer pH 8.0 and diluted with deionized water in 25 mL volumetric flasks. Absorbance of each solution was detected at 490 nm. The results were shown in Table 3.1 and Figure 3.2. It was seen that the absorbance as peak height increased to maximum at concentration of nitroso-R salt was 2.0×10^{-5} mol L^{-1} and then it became constant and so did the absorbance as AU. Therefore, 2.0×10^{-5} mol L^{-1} of nitroso-R salt concentration was chosen.

ลิขสิทธิ์มหาวิทยาลัยเชียงใหม่
Copyright© by Chiang Mai University
All rights reserved

Table 3.1 Effect of nitroso-R salt concentrations for mole-ratio Ni-nitroso-R salt complex

[nitroso-R salt] (x 10 $^{-5}$ mol L^{-1})	**Mole ratio (Ni:nitroso-R salt)**	**Absorbance (AU)***
0.0	1:0	0.004
1.0	1:1	0.121
2.0	1:2	0.242
3.0	1:3	0.242
4.0	1:4	0.243
5.0	1:5	0.243
6.0	1:6	0.244

*average of triplicate results

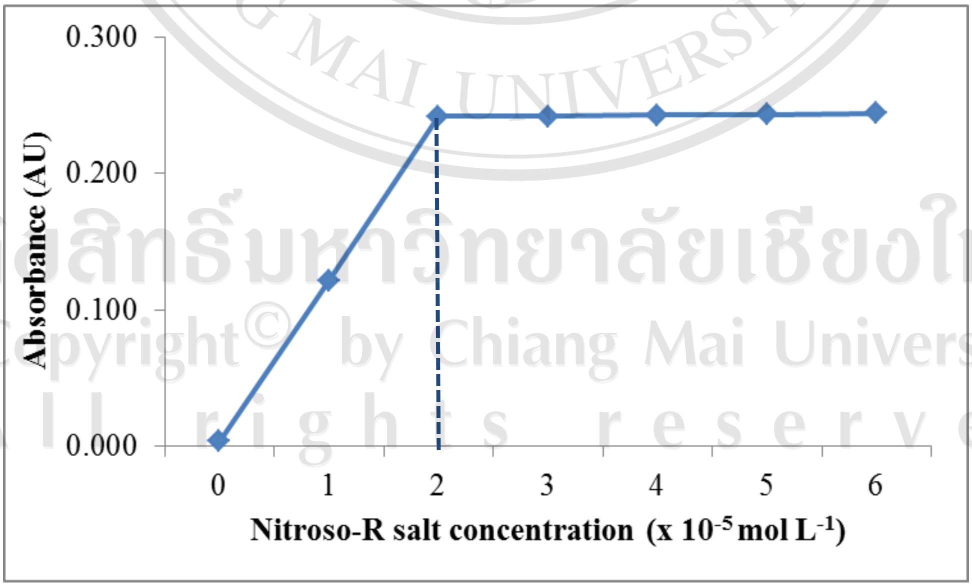

Figure 3.2 Mole-ratio study of Ni(II)-nitroso-R salt system; Ni 1.0×10^{-5} mol L^{-1}, pH 8.0, wavelength 490 nm

ลิขสิทธิ์มหาวิทยาลัยเชียงใหม่
Copyright© by Chiang Mai University
All rights reserved

From experimental results in Tables 3.1 and Figure 3.2 exhibited a mole-ratio of M^{n+} : L was 1:2 (where M^{n+} and L represents metal ions and ligand respectively, indicating that the stoichiometry of the Ni(II)-nitroso-R salt was 1:2). Therefore, the reaction of nickel-nitroso-R salt complex may be exactly the similar as reaction of nickel-nitroso-R salt [260]. The possible complexation reaction of nickel-nitroso-R salt was displayed in Figure 3.3.

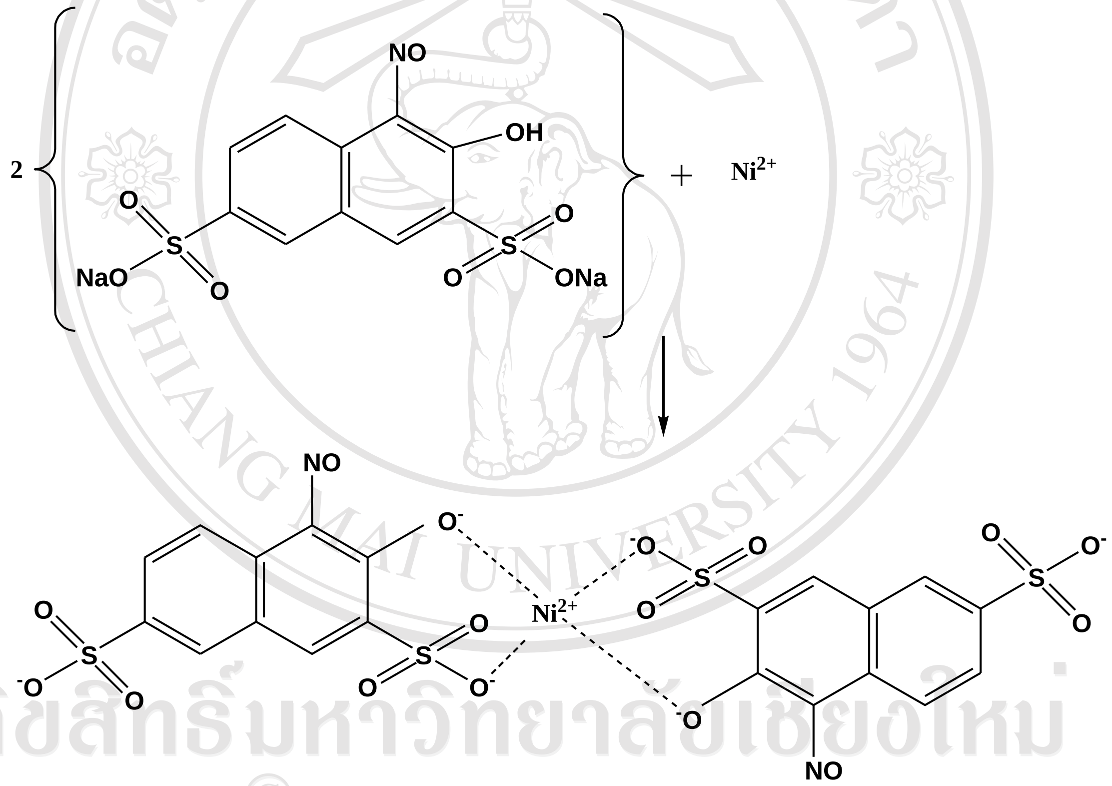

Figure 3.3 The chemical reaction between Ni(II) and nitroso-R salt

ลิขสิทธิ์มหาวิทยาลัยเชียงใหม่
Copyright© by Chiang Mai University
All rights reserved

3.1.3 Design of the flow injection system for Ni(II) determination

The proposed two channels FIA manifold for nickel determination is displayed in Figure 3.4. The system consisted of a six-port selection valve (V) and a peristaltic pump (ISMATEC) (P) which were controlled by “SIA” software programmed in our laboratory to inject accurate volume of samples (S) and transport appropriate flow rate of reagent (R), a PTFE (0.84 mm i.d., 30 cm long) mixing coil was used as reactor (M), a 10 mm path length with 120 μL flow through cell (F) in the cell compartment of the UV-Vis spectrophotometer (Jenway 6305) using as detector (D). A personal computer is used for recording and collecting the absorption signal and controlling the entire system.

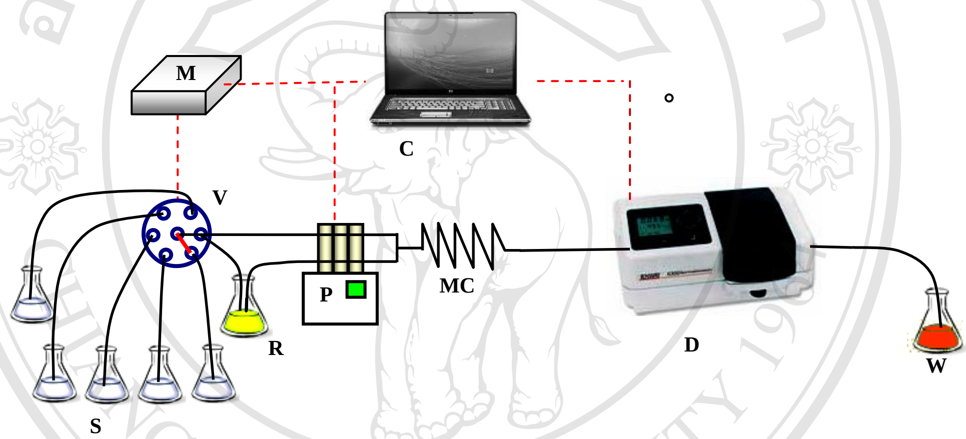

Figure 3.4 The proposed FIA system for nickel determination; S : sample, R : reagent, V : selection valve, M : motor driver unit, P : peristaltic pump, MC : mixing coil, C : personal computer, D : spectrometer and W :waste

ลิขสิทธิ์มหาวิทยาลัยเชียงใหม่
Copyright© by Chiang Mai University
All rights reserved

3.1.4 Optimization of the experimental conditions

The conditions for the determination of Ni(II) were optimized by studying the influences of the various parameters on the FIA gram, such as, pH concentration of nitroso-R salt, flow rate, reaction coil and sample loop, respectively. The optimum conditions obtained by means of the univariate optimization procedure as describes earlier in the experimental section. The optimum values were selected from the maximum sensitivity with low background and standard deviation. The optimizations of the experimental conditions were carried out by using standard Ni(II) solution. In all experiments, five replicate measurements were performed for each studied parameter and the FIA manifold in Figure 3.4 was employed.

3.1.4.1 Effect of pH

Selectivity for spectrophotometric determination of each metal ion can be obtained by adjusting the pH level of the reaction medium. The pH of solution is not only affecting on the selectivity but also influenced on the stoichiometry of the complexes resulting in hypsochromic shift and/or bathochromic shift of the maximum absorption wavelength (λ_{max}) depending on the reaction involves. Therefore, it is necessary to study the effect of pH on the absorbance of the Ni(II)-nitroso-R salt complex. The complexation of Ni(II)-nitroso-R salt was studied at different pH values in the range of 6.5-9.5. The results obtained are displayed in Table 3.2 and Figure 3.5. It was found that at the pH values below 8.5 or above 8.5 the sensitivity (slope of the calibration curve) decreased significantly because at pH 8.5 the complex of Ni(II)-nitroso-R salt might be formed more efficiently than the other pH. In addition, it can be seen that at pH lower and higher than 8.5 the sensitivity of Ni(II)-nitroso-R salt complex decreased due to at pH less than 8.5 the complex of Ni(II)-nitroso-R salt might not be formed effectively, and at pH greater than 8.5 the complex might be decomposed causing a decrease in sensitivity. Therefore, pH 8.5 was chosen because it provided the greatest sensitivity.

ลิขสิทธิ์มหาวิทยาลัยเชียงใหม่
Copyright© by Chiang Mai University
All rights reserved

Table 3.2 Effect of pH on the sensitivity

pH	Peak height* (AU) obtained from the standard Ni(II) (mg L^{-1})					y = mx + c	r^2
	0.50	1.0	1.5	2.0	2.5		
6.5	0.014	0.025	0.038	0.050	0.059	0.0116x + 0.0024	0.9979
7.0	0.025	0.036	0.046	0.059	0.076	0.0249x + 0.0112	0.9899
7.5	0.037	0.045	0.065	0.075	0.096	0.0290x + 0.0199	0.9797
8.0	0.040	0.057	0.075	0.091	0.103	0.0318x + 0.0256	0.9939
8.5	0.047	0.063	0.077	0.093	0.116	0.0339x + 0.0286	0.9906
9.0	0.033	0.047	0.055	0.065	0.082	0.0230x + 0.0218	0.9836
9.5	0.073	0.072	0.073	0.073	0.073	0.0209x + 0.0186	0.9969

*average of five replicate results

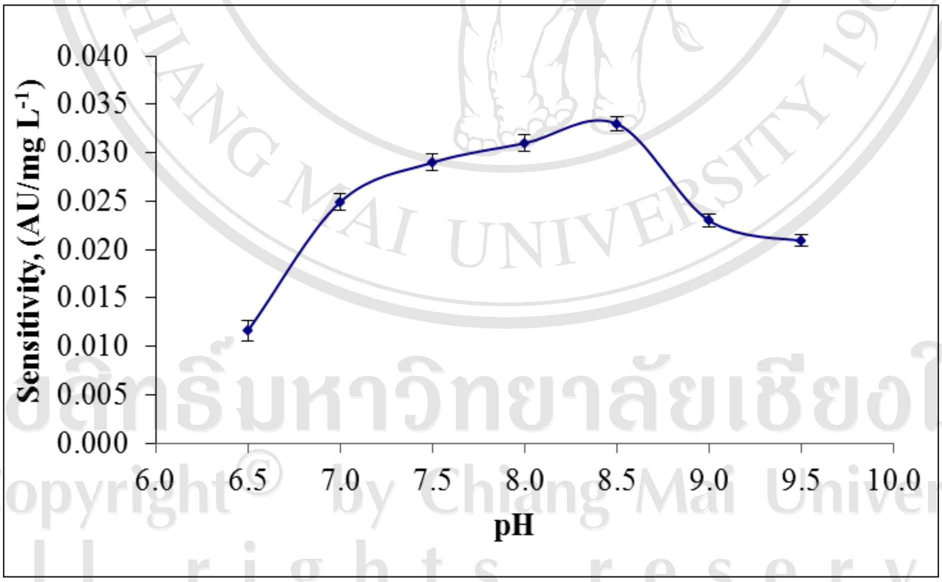

Figure 3.5 Relationship between pH and the sensitivity of the calibration curve

ลิขสิทธิ์มหาวิทยาลัยเชียงใหม่
Copyright© by Chiang Mai University
All rights reserved

3.1.4.2 Effect of nitroso-R salt concentrations

Commonly, the concentration of reagent was greater than required stoichiometry of the complex (Ni(II) : nitroso-R salt = 1:2) was demanded for complete color development. Effect of nitroso-R salt concentrations on the determination of Ni(II) (0.5-2.5 mg L^{-1}) was investigated over the range of 0.0026 – 0.0208 mol L^{-1}. The results are displayed in Table 3.3 and Figure 3.6. The absorbance increased with increasing concentrations of nitroso-R salt from 0.0026 to 0.0104 mol L^{-1}, above which the absorbance slightly decreased (Figure 3.6). Results show that nitroso-R salt concentration must be exceed that of Ni(II) ion concentration to reach effective complexation to achieve high sensitivity (slope of the calibration curve). As a result the optimum concentration of nitroso-R salt was 0.0104 mol L^{-1}.

Table 3.3 Effect of nitroso-R salt concentration on the sensitivity of Ni(II)-nitroso-R salt complex

Nitroso-R salt (x 10^{-2} mol L^{-1})	**Peak height * (AU) obtained from the standard Ni(II) (mg L^{-1})**					**y = mx + c**	**r^2**
	0.50	**1.0**	**1.5**	**2.0**	**2.5**		
0.26	0.015	0.019	0.030	0.039	0.054	y = 0.0198x + 0.0017	0.9862
0.52	0.019	0.027	0.039	0.055	0.069	y = 0.0253x - 0.0039	0.9860
0.78	0.027	0.038	0.056	0.069	0.084	y = 0.0288x - 0.0117	0.9979
1.04	0.039	0.055	0.068	0.085	0.105	y = 0.0323x + 0.0220	0.9954
1.30	0.050	0.069	0.084	0.100	0.111	y = 0.0307x - 0.0369	0.9919
1.56	0.063	0.081	0.100	0.111	0.121	y = 0.0292x + 0.0516	0.9797
1.82	0.081	0.095	0.111	0.124	0.137	y = 0.0280x + 0.0675	0.9982
2.08	0.084	0.110	0.123	0.136	0.143	y = 0.0289x - 0.0758	0.9516

*average of five replicate results

ลิขสิทธิ์มหาวิทยาลัยเชียงใหม่
Copyright© by Chiang Mai University
All rights reserved

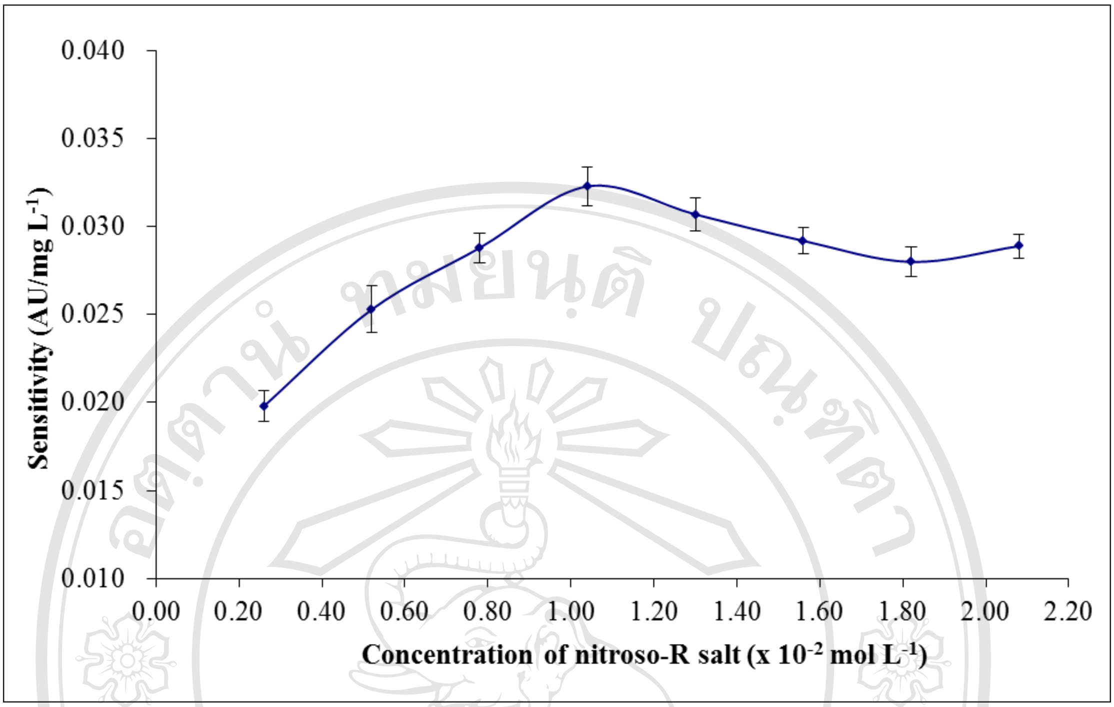

Figure 3.6 Effect of nitroso-R salt concentration on the sensitivity of Ni(II)-nitroso-R salt complex

3.1.4.3 Effect of the reaction coil tubing length

The reaction coil are important for confirming complete reagent combining consequent in a time delay for development of a reaction between Ni(II) and nitroso-R salt. This condition was investigated by using PTFE tubing with diameter of 1.07 mm i.d. and length of reaction coil was varied from 10 to 50 cm. The 0.0104 mol L^{-1} nitroso-R salt and 0.5 mol L^{-1} ammonium acetate buffer pH 8.5 were employed as reagent streams. The total flow rate of reagents was 2.0 mL min^{-1}. The results are displayed in Table 3.4 and Figure 3.7. The sensitivity increased to a maximum at a reaction coil tubing length of 30 cm. It can be described that increasing the reaction coil length up to 30 cm give rise to an increase in the residence time permitting well

ลิขสิทธิ์มหาวิทยาลัยเชียงใหม่
Copyright© by Chiang Mai University
All rights reserved

mixing between Ni(II) and nitroso-R salt. Therefore, the reaction coil length 30 cm was chosen as optimum since it provided the greatest sensitivity.

Table 3.4 Effect of reaction coil length on the sensitivity

Reaction coil length (cm)	Peak height* (AU) obtained from the standard Ni(II) (mg L^{-1})					y = mx + c	r^2
	0.50	**1.0**	**1.5**	**2.0**	**2.5**		
10	0.035	0.050	0.070	0.088	0.115	y = 0.0395x + 0.0124	0.9897
20	0.038	0.053	0.076	0.101	0.117	y = 0.0411x + 0.0154	0.9923
30	0.042	0.064	0.084	0.107	0.127	y = 0.0427x + 0.0207	0.9995
40	0.036	0.058	0.072	0.092	0.109	y = 0.0359x + 0.0195	0.9973
50	0.037	0.056	0.070	0.087	0.107	y = 0.0342x + 0.0201	0.9981

*average of five replicate results

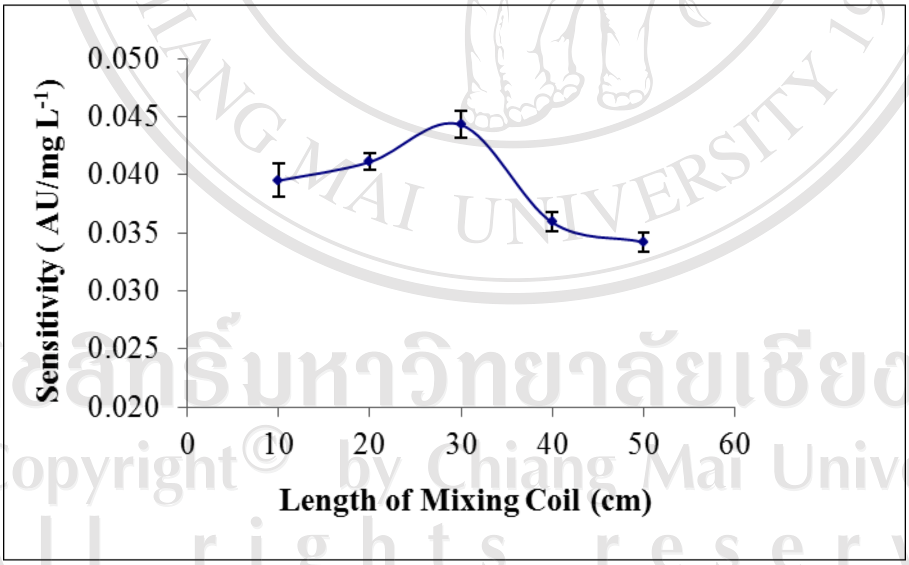

Figure 3.7 Effect of the coil length on the sensitivity of Ni(II)-nitroso-R salt complex

ลิขสิทธิ์มหาวิทยาลัยเชียงใหม่
Copyright© by Chiang Mai University
All rights reserved

3.1.4.4 Effect of flow rate

Flow rates can be affecting on the FIA signals due to dispersion zone process. A high flow rate leads to the shorter time for each sample passing through the detector and a low precision of the peak height and a high rate of reagent consumption. With a low flow rate, the residence time for each sample is long and the dispersion zone is large which can reduce the sensitivity and the sample throughput. Therefore, the effects of total flow rates on absorption signal of Ni(II)-nitroso-R complex in the FIA system were investigated for determining nickel, by injecting various concentration of standard nickel solution (0.5 - 2.5 mg L^{-1}) into the flow system. Flow rates were varied from 1.0 to 5.0 mL min^{-1}. The effect of flow rate on the sensitivity was displayed in Table 3.5 and Figure 3.8. It can be seen that the optimum flow rate was 2.5 ml min^{-1}. Moreover, the sensitivity of the calibration curve decreased, when the flow rate was lower than 2.5 ml min^{-1}. Due to the low flow rate increased in dispersion zone process and hence, peak broadening was observed. Furthermore, the sensitivity of the calibration curve was poorer when the flow rate was higher than 2.5 ml min^{-1}. This is due to the fact that the higher flow rate reduced the reaction time and so inadequate complex formation.

ลิขสิทธิ์มหาวิทยาลัยเชียงใหม่
Copyright© by Chiang Mai University
All rights reserved

Table 3.5 Effect of flow rate on the sensitivity

Flow rate (mL min^{-1})	Peak height* (AU) obtained from the standard Ni(II) (mg L^{-1})					y = mx + c	r^2
	0.50	1.0	1.5	2.0	2.5		
1.0	0.035	0.050	0.070	0.088	0.115	y = 0.0396x + 0.0122	0.9897
1.5	0.038	0.053	0.076	0.101	0.117	y = 0.0412x + 0.0152	0.9929
2.0	0.040	0.064	0.084	0.107	0.122	y = 0.0414x + 0.0213	0.9948
2.5	0.037	0.058	0.077	0.098	0.124	y = 0.0428x + 0.0146	0.9967
3.0	0.037	0.056	0.073	0.095	0.119	y = 0.0406x + 0.0151	0.9954
3.5	0.035	0.052	0.072	0.091	0.115	y = 0.0398x + 0.0133	0.9965
4.0	0.033	0.049	0.070	0.089	0.110	y = 0.0388x + 0.0120	0.9981
4.5	0.032	0.050	0.070	0.086	0.106	y = 0.0368x + 0.0136	0.9991
5.0	0.030	0.048	0.067	0.085	0.101	y = 0.0358x + 0.0125	0.9992

*average of five replicate results

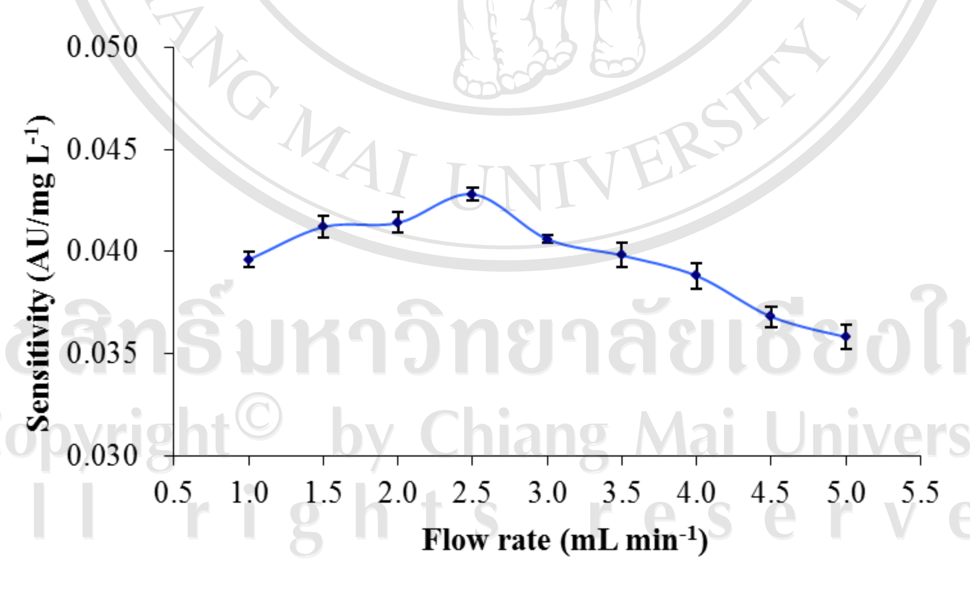

Figure 3.8 Effect of flow rate on the sensitivity of Ni(II)-nitroso-R salt complex

ลิขสิทธิ์มหาวิทยาลัยเชียงใหม่
Copyright© by Chiang Mai University
All rights reserved

3.1.4.5 Effect of sample introduction volume

The sample/nickel volume injected into the nitroso-R salt stream has an important effect on sensitivity. The effect of sample volume on the determination of 0.5-2.5 mg L^{-1} Ni(II) that the influence on Ni(II)-nitroso-R complex absorption was studied by controlling pump flow rate and changing the switching time of the selection valve at sample line over the range of 50, 60, 70, 80, 90 and 100 μL. The results are displayed with sensitivity in Table 3.6 and Figure 3.9. It was found that the sensitivity increases with rising sample volume up to 80 μL due to the enhancement in sample volume leading to the increment of the quantity of complex (Ni(II)-nitroso R salt), that cause increases in peak height. Hereafter, the injection volume of 80 μL was considered to be optimum sample introduction volume for the proposed FIA system, which was used throughout the next experiments.

Table 3.6 Effect of sample volume on the sensitivity

Sample volume (μL)	**Peak height * (AU) obtained from the standard Ni(II) (mg L^{-1})**					**y = mx + c**	**r^2**
	0.50	**1.0**	**1.5**	**2.0**	**2.5**		
50	0.037	0.057	0.070	0.094	0.110	y = 0.0369x + 0.0185	0.9951
60	0.040	0.065	0.082	0.101	0.118	y = 0.0383x + 0.0239	0.9950
70	0.047	0.076	0.095	0.115	0.130	y = 0.0381x + 0.0042	0.9856
80	0.049	0.076	0.102	0.121	0.137	y = 0.0442x + 0.0307	0.9875
90	0.047	0.075	0.096	0.119	0.135	y = 0.0440x + 0.0284	0.9920
100	0.045	0.075	0.094	0.120	0.132	y = 0.0438x + 0.0275	0.9830

* average of five replicate results

ลิขสิทธิ์มหาวิทยาลัยเชียงใหม่
Copyright© by Chiang Mai University
All rights reserved

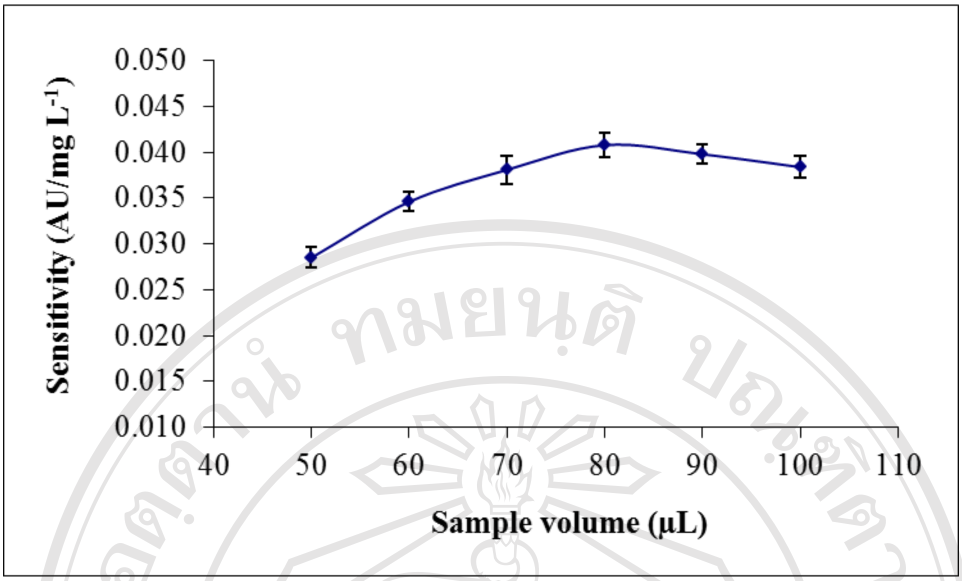

Figure 3.9 Effect of sample introduction volume on the sensitivity of Ni(II)-nitroso-R complex

3.1.5 Analytical Characteristics

3.1.5.1 Linear range

The linear range of the proposed method was investigated by flowing Ni(II) standard solution into FI system under the suitable conditions that were studied previously. Linear range of the calibration graph was found for Ni(II) standards at the concentration ranging from 0.25–3.5 mg L^{-1}. All measurements were made in five replication injections. The results obtained are displayed in Table 3.7 and Figure 3.10.

ลิขสิทธิ์มหาวิทยาลัยเชียงใหม่
Copyright© by Chiang Mai University
All rights reserved

Table 3.7 Peak height at various Ni(II) concentrations for linearity inspect of the calibration graph

Ni(II) (mg L^{-1})	**Peak height (AU)** *					**$\bar{x}$**	**SD**
	1	**2**	**3**	**4**	**5**		
0.10	0.016	0.016	0.015	0.016	0.015	0.016	0.0005
0.25	0.026	0.026	0.027	0.026	0.025	0.026	0.0007
0.30	0.030	0.029	0.028	0.029	0.029	0.029	0.0007
0.40	0.035	0.035	0.034	0.035	0.034	0.035	0.0005
0.50	0.040	0.039	0.039	0.040	0.039	0.039	0.0005
0.60	0.045	0.043	0.044	0.045	0.044	0.044	0.0008
0.70	0.050	0.047	0.049	0.048	0.049	0.049	0.0011
0.80	0.054	0.054	0.054	0.053	0.054	0.054	0.0004
0.90	0.058	0.061	0.062	0.059	0.061	0.060	0.0016
1.0	0.063	0.065	0.067	0.063	0.065	0.065	0.0017
1.1	0.068	0.069	0.072	0.067	0.069	0.069	0.0019
1.2	0.073	0.073	0.075	0.071	0.075	0.073	0.0017
1.3	0.078	0.077	0.080	0.075	0.079	0.078	0.0019
1.4	0.083	0.081	0.085	0.079	0.083	0.082	0.0023
1.5	0.088	0.085	0.090	0.083	0.087	0.087	0.0027
1.6	0.093	0.089	0.095	0.087	0.091	0.091	0.0032
1.7	0.098	0.093	0.100	0.091	0.095	0.095	0.0036
1.8	0.103	0.097	0.105	0.095	0.099	0.100	0.0041
1.9	0.108	0.101	0.110	0.099	0.103	0.104	0.0047
2.0	0.112	0.106	0.114	0.104	0.107	0.109	0.0042
2.1	0.116	0.111	0.118	0.109	0.111	0.113	0.0038
2.2	0.120	0.116	0.122	0.114	0.115	0.117	0.0034
2.3	0.124	0.121	0.126	0.119	0.119	0.122	0.0031
2.4	0.128	0.126	0.130	0.124	0.123	0.126	0.0029
2.5	0.132	0.131	0.134	0.129	0.127	0.131	0.0027
2.6	0.136	0.136	0.138	0.134	0.131	0.135	0.0026
2.7	0.140	0.141	0.142	0.139	0.135	0.139	0.0027
2.8	0.144	0.146	0.146	0.144	0.139	0.144	0.0029

ลิขสิทธิ์มหาวิทยาลัยเชียงใหม่
Copyright© by Chiang Mai University
All rights reserved

Table 3.7 (continued)

Ni(II) (mg L^{-1})	Peak height (AU) *					$\bar{x}$	SD
	1	2	3	4	5		
2.9	0.148	0.151	0.150	0.149	0.143	0.148	0.0031
3.0	0.152	0.156	0.154	0.154	0.147	0.153	0.0034
3.1	0.156	0.161	0.158	0.159	0.151	0.157	0.0038
3.2	0.160	0.166	0.162	0.167	0.155	0.162	0.0048
3.3	0.164	0.171	0.166	0.172	0.159	0.166	0.0053
3.4	0.168	0.175	0.170	0.176	0.163	0.170	0.0053
3.5	0.176	0.178	0.178	0.177	0.177	0.177	0.0008
3.6	0.186	0.187	0.186	0.187	0.187	0.187	0.0005
3.7	0.208	0.207	0.208	0.209	0.209	0.208	0.0008

* average of five replicate results

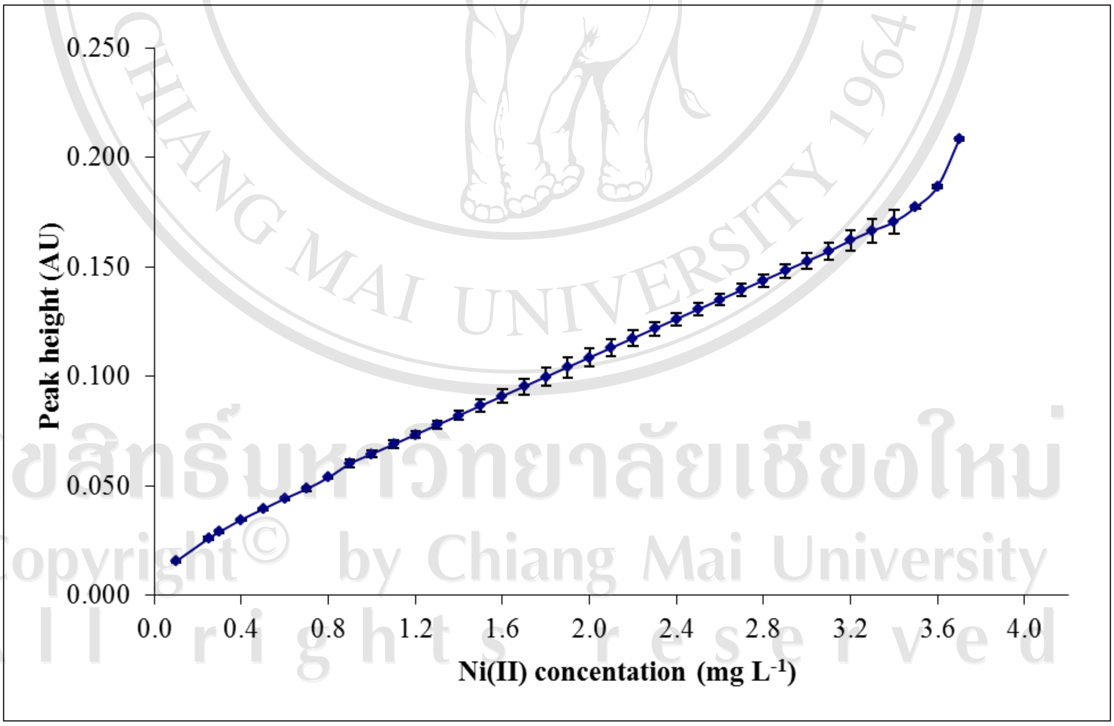

Figure 3.10 Relationship between peak height and concentrations of Ni(II)

ลิขสิทธิ์มหาวิทยาลัยเชียงใหม่
Copyright© by Chiang Mai University
All rights reserved

3.1.5.2 Precision and accuracy of the proposed method

The precision of the proposed method was verified by 11 replicated determination of 1.0 mg L^{-1} standard Ni(II), underneath the optimum conditions. The relative standard deviation (RSD) was found to be 1.76% (Table 3.8). Moreover, the percentage recoveries were studied by spiking 0.5 mg L^{-1} of Ni(II) standard solution into water samples (Table 3.13) for checking accuracy of this method. It was found that the range of percentage recovery was calculated to be 98.3-101.8 % (n=3).

Table 3.8 Precision of verification using standard 1.0 mg L^{-1} Ni(II)

Experimental number	**Peak height (AU)***
1	0.060
2	0.061
3	0.061
4	0.062
5	0.061
6	0.062
7	0.059
8	0.062
9	0.061
10	0.059
11	0.061
$\overline{X}$	0.061
SD	0.0011
% RSD	1.76

*average of five replicate results

ลิขสิทธิ์มหาวิทยาลัยเชียงใหม่
Copyright© by Chiang Mai University
All rights reserved

3.1.5.3 Calibration curve

A calibration curve was accomplished by injecting Ni(II) standard solutions into the proposed FIA system under the optimum conditions. All measurements were made in five replicate injections (Figure 3.11). These results were displayed in Table 3.9. The calibration curve (Figure 3.12) was linear over the range 0.25-3.5 mg L^{-1} and the linear regression equation of $y = 0.0458x + 0.0144$, where y is absorbance of Ni(II)-nitroso-R complex and x is the concentration of Ni(II) in mg L^{-1}. The correlation coefficient for this line was 0.9998.

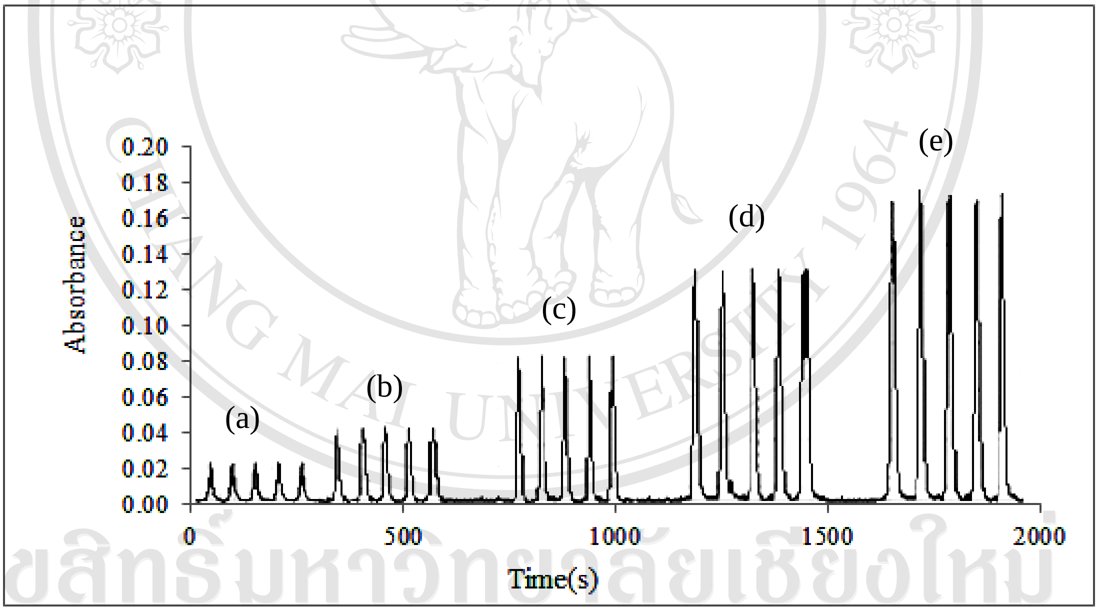

Figure 3.11 FIA-gram of standard Ni(II) solution at (a) 0.25 mg L^{-1}, (b) 0.5 mg L^{-1}, (c) 1.5 mg L^{-1}, (d) 2.5 mg L^{-1} and (e) 3.5 mg L^{-1} respectively

ลิขสิทธิ์มหาวิทยาลัยเชียงใหม่
Copyright© by Chiang Mai University
All rights reserved

Table 3.9 The absorbance of Ni(II)-nitroso-R salt complex for calibration curve

Ni(II)	**Peak height (AU)***						
(µg mL^{-1})	**1**	**2**	**3**	**4**	**5**	**$\bar{x}$**	**SD**
0.25	0.026	0.025	0.026	0.024	0.024	0.025	0.0001
0.50	0.038	0.039	0.038	0.037	0.038	0.038	0.0007
1.50	0.085	0.083	0.085	0.084	0.083	0.084	0.0010
2.50	0.131	0.128	0.130	0.129	0.123	0.1282	0.0031
3.50	0.176	0.174	0.177	0.175	0.173	0.175	0.0016

* average of five replicate results

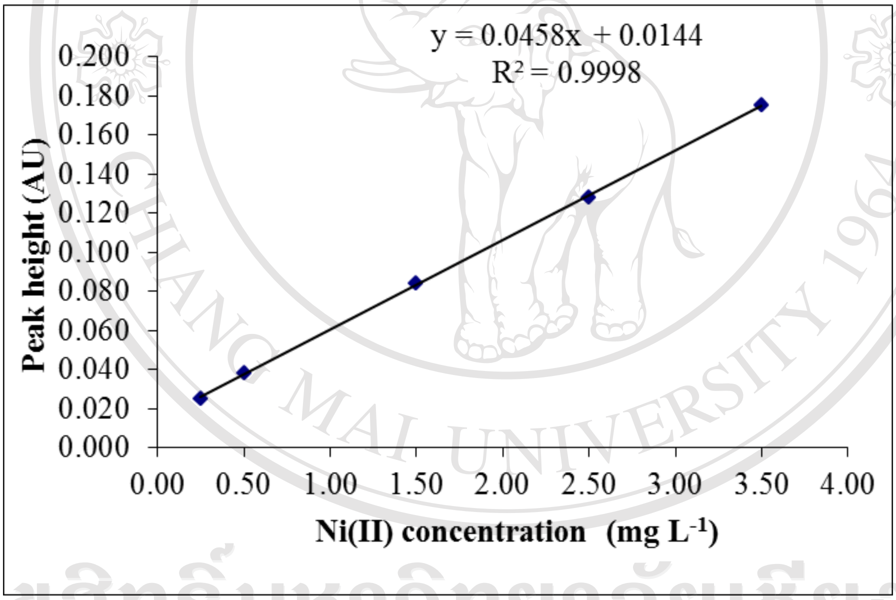

Figure 3.12 Calibration curve for Ni(II) determination using the FIA system

ลิขสิทธิ์มหาวิทยาลัยเชียงใหม่
Copyright© by Chiang Mai University
All rights reserved

3.1.5.4 Detection limit [259]

The detection limit was determined by the method as defined by Miller [259] which was calculated from the linear regression line of calibration curve of the analyte. The results are giving in Tables 3.10. The concentration at limit of detection can be calculated from equation 2.3-2.4. It was found that the LOD of the proposed FIA was 0.081 mg L^{-1} and LOQ was 0.272 mg L^{-1}. The sample throughput was 80 h^{-1}.

Table 3.10 Calculation of detection limit of FIA spectrophotometric for Ni(II) determination

Ni(II) (mg L^{-1})	Y_i^*	$\hat{Y}_i$	$\lvert Y_i^* - \hat{Y}_i \rvert$	$\lvert Y_i^* - \hat{Y}_i \rvert^2$
0.25	0.025	0.026	0.001	1.0×10^{-6}
0.5	0.038	0.037	0.001	1.0×10^{-6}
1.5	0.084	0.083	0.001	1.0×10^{-6}
2.5	0.1282	0.129	0.0008	6.4×10^{-7}
3.5	0.175	0.174	0.001	1.0×10^{-6}
$\sum(\lvert Y_i^* - \hat{Y}_i \rvert^2)$				4.64×10^{-6}
S_y/x				1.244×10^{-3}
C_L, LOD				0.08
LOQ				0.27

ลิขสิทธิ์มหาวิทยาลัยเชียงใหม่
Copyright© by Chiang Mai University
All rights reserved

The linear regression equation is Y = 0.0458x + 0.0144

$$Sy/x = [4.64 \times 10^{-6}/(5-2)]^{1/2}$$

$$= 1.244 \times 10^{-3}$$

$$C_L, \text{LOD} = (3 \times 1.244 \times 10^{-3})/0.0458$$

$$= 0.08 \text{ mg L}^{-1} \text{ Ni(II)}$$

$$LOQ = (10 \times 1.244 \times 10^{-3})/0.0458$$
$$= 0.27 \text{ mg L}^{-1} \text{ Ni(II)}$$

3.1.5.5 Interference studies

The effect of various ions on the determination of 1.0 μg mL^{-1} Ni(II) was considered according to the procedure described earlier. The tolerance limit of an ion was taken as the maximum amount (μg mL^{-1}) causing an error not greater than 10% in the concentration of analytes [50]. Table 3.11 displayed that, most ions studied did not interfere with the determination of Ni(II). The tolerance concentrations were studied species to 1.0 μg ml^{-1} Ni(II) under the optimum conditions. It was found that Na^{+}, K^{+}, Ca^{2+}, Ba^{2+}, NO_3^{-}, NO_2^{-} and SO_4^{2-} did not interfere when present up to 200 μg mL^{-1}. Al^{3+}, Cr^{3+}, Mg^{2+}, Cl^{-} and PO_4^{3-} did not have any effect up to 100 μg mL^{-1}. Mn^{2+} was tolerated up to 80-fold excess. In addition, Pb^{2+}, Cd^{2+} and Zn^{2+} were permitted up to 30-fold excess. However, Fe^{3+}, Co^{2+} and Cu^{2+} were strongly interfered when they present more than 1-fold excess. Fe^{3+} were exist in the water samples in several μg mL^{-1} and need to be eliminated prior to analysis of Ni(II) by using 4.0% sodium fluoride as masking agent. Moreover, Co^{2+} can be eliminated by using 1.0% potassium oxalate solution as marking agent and Cu^{2+} was masked with 0.30% thiourea. The studied marking agents were displayed in Table 1E (appendix E).

ลิขสิทธิ์มหาวิทยาลัยเชียงใหม่
Copyright© by Chiang Mai University
All rights reserved

Table 3.11 Tolerable levels of interferences ions effect on the signal obtained from 1.0 μg mL^{-1} Ni(II)

Interference ion	**Tolerable concentration ratio[a] (μg mL^{-1}) ions/1.0 μg mL^{-1} Ni(II)**
Na^+, K^+, Ca^{2+}, Ba^{2+}, NO_3^-, NO_2^-, SO_4^{2-}	200
Al^{3+}, Cr^{3+}, Mg^{2+}, Cl^-, PO_4^{3-}	100
Mn^{2+}	80
Pb^{2+}, Cd^{2+}, Zn^{2+}	30
Co^{2+}	20 ([b])
Cu^{2+}	20 ([c])
Fe^{3+}	15 ([d])

[a] The foreign species concentration causing error smaller than ±10% for request to the signal Ni(II) alone

[b] 1.0% oxalate as masking agent

[c] 0.20% thiourea as masking agent

[d] 4.0% sodium fluoride as masking agent

In addition, a diagram of the designed FIA manifold is used in Figure 3.4. Table 3.12 displays the ranges over which the variables involved in the FIA system were studied and their optimum values. Moreover, Table 3.12 summarizes the analytical characteristics for determination of nickel.

ลิขสิทธิ์มหาวิทยาลัยเชียงใหม่
Copyright © by Chiang Mai University
All rights reserved

Table 3.12 The Optimum conditions and the analytical characteristics for Ni(II) determination with the FIA system

Parameters	Studied range	Optimized value
Injection volume (μL)	50-100	80
Flow rate (mL min^{-1})	1.0-5.0	2.5
Nitroso-R salt concentration (x 10^{-2} mol L^{-1})	0.26-2.08	1.04
pH	6.5-9.5	8.5
Wave length (nm)	400-700	490
Reaction coil length (cm)	10-50	30
Linear range (mg L^{-1})	0.10-3.7	0.25-3.5
Correlation coefficients (r^2)	-	0.9998
RSD (n=11)	-	1.76
LOD (mg L^{-1})	-	0.08
LOQ (mg L^{-1})	-	0.27

3.1.6 Determination of Ni(II) in water samples

Following the procedure described in the previous sections, the proposed method was applied to the determination of Ni(II) in water samples (E1-E8) which were collected from electroplating and electronic industry with different time in Lam Phun Province, Thailand, where the Northern Industrial Estate was located . The results are given in Table 3.13 compared with those obtained by FAAS. The results obtained by the proposed FI spectrophotometric method compared favorably with those obtained by FAAS (Table 3.14) using the student *t*-test (appendix C). It was seen that experimental *t*-value for Ni(II) assay, which was smaller than the theoretical *t*-value at a confidence interval of 95% (4.30) indicating that results obtained by both methods were in excellent agreement.

ลิขสิทธิ์มหาวิทยาลัยเชียงใหม่
Copyright© by Chiang Mai University
All rights reserved

The amounts of Ni(II) in water samples analyzed by the proposed FIA method were in the range of 0.281-0.506 mg L^{-1}. With admiration to the amounts of chemical and reagents consumption, the proposed FIA system consumed smaller amount of chemical solution and reagent than those consumed by the batch-wise methods.

Table 3.13 Concentrations of Ni(II) in water samples analyzed by using the proposed FIA system

Water samples	**Ni(II) found (mg L^{-1})**				**SD**	**Ni(II) concentration* (mg L^{-1})**	**% Recovery**
	1	**2**	**3**	**$\bar{x}$**			
E1	0.282	0.275	0.285	0.281	0.005	0.281 ± 0.005	98.55
E2	0.401	0.395	0.396	0.397	0.003	0.397 ± 0.003	99.21
E3	0.312	0.31	0.302	0.308	0.004	0.308 ± 0.004	101.8
E4	0.432	0.439	0.431	0.434	0.004	0.434 ± 0.004	100.1
E5	0.372	0.369	0.371	0.371	0.001	0.371 ± 0.001	98.3
E6	0.445	0.448	0.446	0.446	0.001	0.446 ± 0.001	99.2
E7	ND**	ND**	ND**	-	-	ND**	100.8
E8	0.502	0.505	0.512	0.506	0.004	0.506 ± 0.004	99.69

*average of triplicate results

**not detected

ลิขสิทธิ์มหาวิทยาลัยเชียงใหม่
Copyright © by Chiang Mai University
All rights reserved

Table 3.14 Comparative determination of Ni(II) in water samples by proposed FIA and FAAS

Water sample	**Concentrations (mg L^{-1})**		$t_{calculated}$
	FIA*	**FAAS***	
E1	0.281	0.273	3.169
E2	0.397	0.402	-3.080
E3	0.308	0.315	-2.806
E4	0.434	0.442	-3.893
E5	0.371	0.373	-3.240
E6	0.446	0.449	-3.703
E7	ND**	ND**	-
E8	0.506	0.497	3.858

*average of triplicate results

**not detected

ลิขสิทธิ์มหาวิทยาลัยเชียงใหม่
Copyright© by Chiang Mai University
All rights reserved

3.2 Mini-CNC machine modification with diode laser for rapid fabrication of PMMA chips

The research in this section was aimed at modification of the home-made mini-CNC machine (previously designed and fabricated for fabrication of micro electronic circuit on chip) by coupling with diode laser to obtain a new modified mini-CNC machine for fabrication of PMMA chips. Application of the fabricated PMMA chips as micro reactors in μFA manifolds were also encountered.

3.2.1 Mini-CNC machine modification with diode laser

Figure 3.13 displayed the complete mini-CNC machine modified with diode laser for fabrication of PMMA chips. The maximum power of diode laser was 5 W at wavelength 808 nm near infrared region. The scanning speed was 1.0-10.0 mm s^{-1} by the combined moving of X-Y stages.

3.2.2 Design and fabrication of the PMMA chip

The mini-CNC machine was successfully modified with diode laser for fabrication of a PMMA chip. The power of laser diode is controlled by the pulse width modulator. The position of laser diode is placed at Z-direction on mini-CNC. The movement of combined X-Y stage was achieved commands by KCAM program. The designed patterns were sent onto KCAM program to control the fabrication of microchannel on a PMMA sheet. The patterns of PMMA chip is designed with computer program as shown in Figure 3.14, resulting the complete PMMA microchannel in Figure 3.15. The important point was the combination of lines that they should be complete connected due to the discontinuous movement of the operating of fabrication microchannel resulting in rough channel. Figure 3.15 was

ลิขสิทธิ์มหาวิทยาลัยเชียงใหม่
Copyright© by Chiang Mai University
All rights reserved

displayed the T-junction with U-turns channel by the length of 2, 10, 20 and 30 cm of microchannels according to design with the computer drawing program.

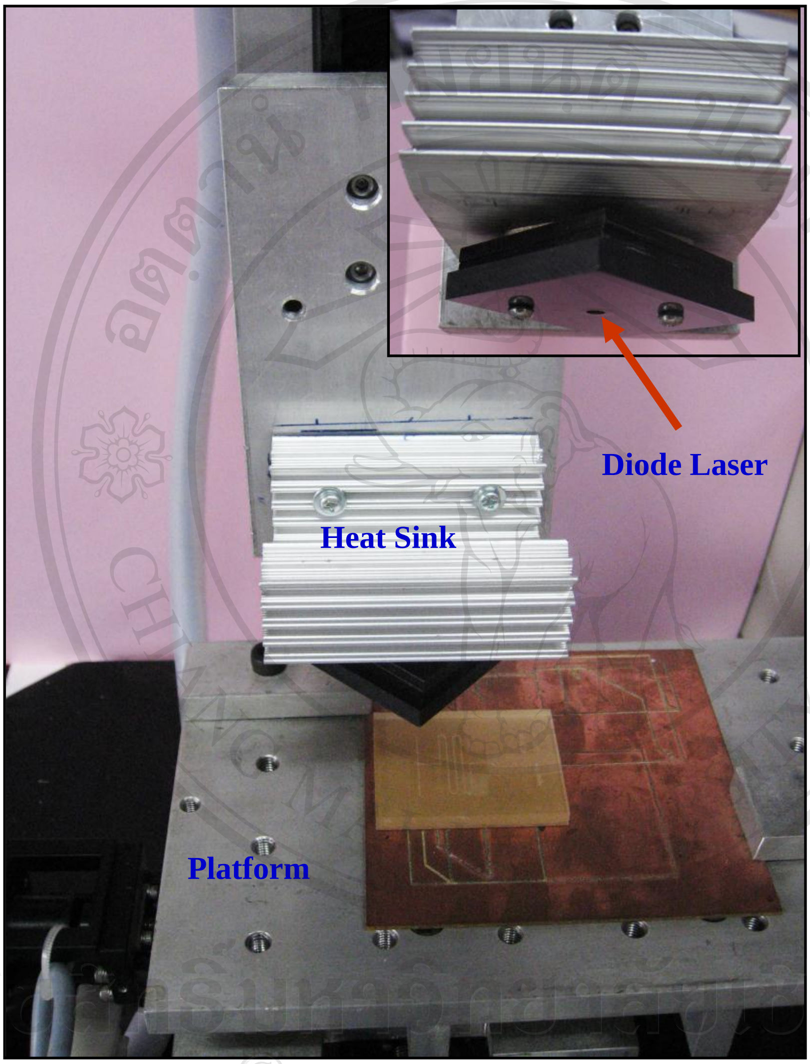

ลิขสิทธิ์มหาวิทยาลัยเชียงใหม่
Copyright© by Chiang Mai University
All rights reserved

Figure 3.13 The diode laser mini-CNC machine system

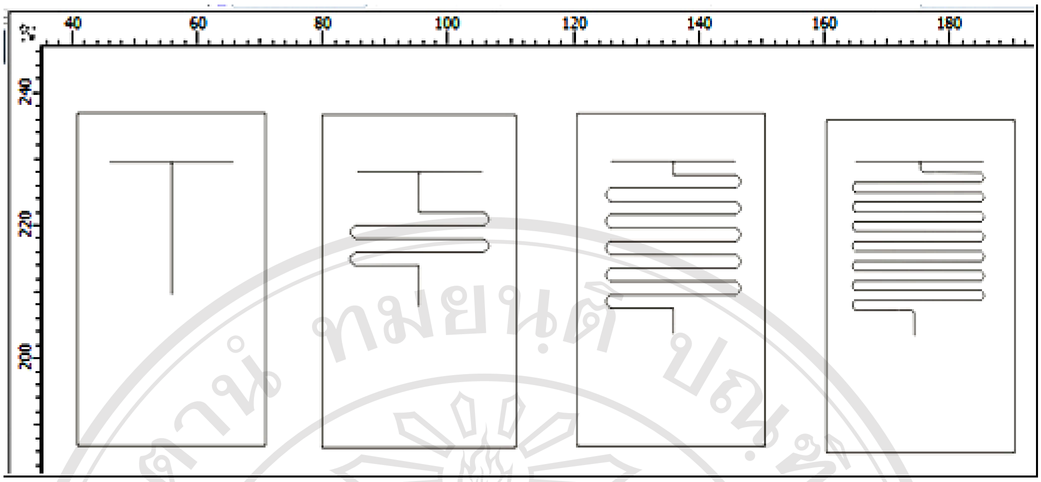

Figure 3.14 The microchannel patterns are designed from Drawing program

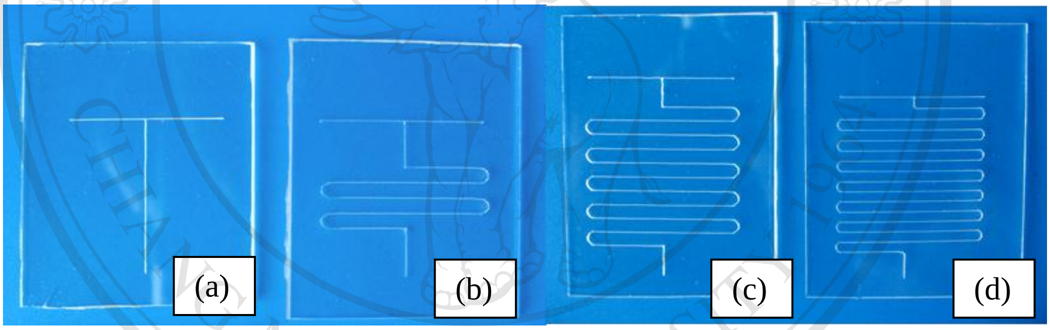

Figure 3.15 The complete PMMA chips make from mini-CNC machine modified with diode laser and the length of microchannels; (a):2 cm, (b): 10 cm, (c): 20 cm, (d): 30 cm

ลิขสิทธิ์มหาวิทยาลัยเชียงใหม่
Copyright© by Chiang Mai University
All rights reserved

3.2.3 The depth and the width of PMMA microchannel

When the focused laser beam exposes to the surface of PMMA, the temperature of the exposed area rises so quickly that the PMMA is first melted, then decomposed and vaporized, leaving a hollow in the PMMA. It means the combined moving X-Y stages driven by the step of motors that is able to cut PMMA. The depth and the width of microchannel were measured using the SEM by cross-sections of microchannel. Preliminary studied the depth of channel using the different speed of X-Y stages. Figure 3.16 displayed three SEM images of a PMMA chips with different depth produced using the diode laser with constant laser energy of 5 W and X-Y movement with the rate of (a) 1.0, (b) 2.0 and (c) 3.0 mm s^{-1}. It was found that the groove depth decreases with an increasing movement speed. Moreover, the different widths of the grooves were created with a constant scanning speed of 4.0 mm s^{-1} and laser power of (a) 3.5 W, (b) 4.0 W and (c) 4.5 W as shown in Figure 3.17. The SEM images close up view was displayed that the widths of the groove expand with increasing in laser energy.

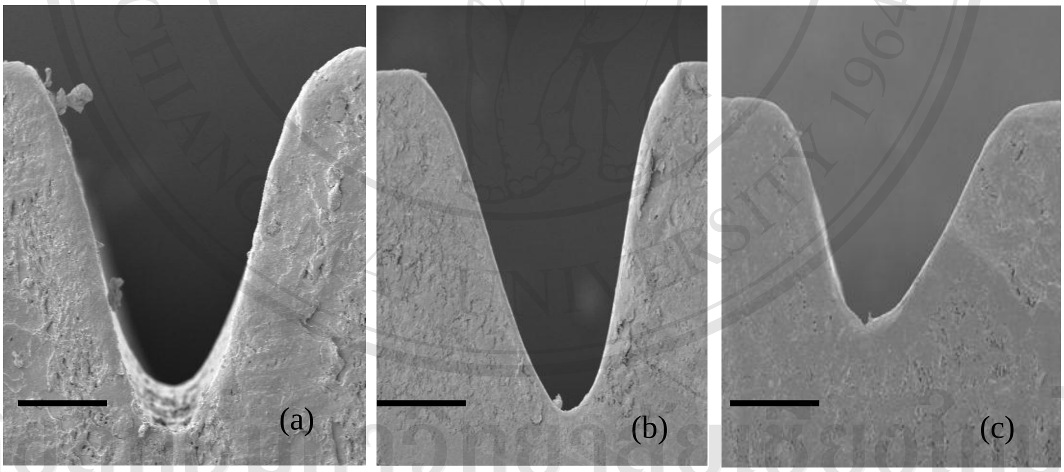

Figure 3.16 SEM images of PMMA chips with different depths of channels using movement speed of (a) 1.0, (b) 2.0 and (c) 3.0 mm s^{-1} (power 5 W)

ลิขสิทธิ์มหาวิทยาลัยเชียงใหม่
Copyright© by Chiang Mai University
All rights reserved

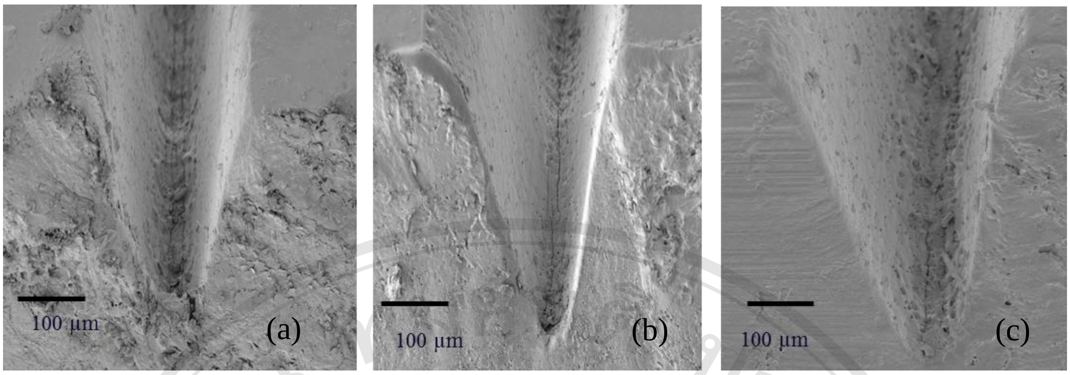

Figure 3.17 SEM images of PMMA substrates with different width of channels using laser power of (a) 3.5 W, (b) 4.0 W and (c) 4.5 W (speed 4 mm s^{-1})

The geometry of the microchannels can be explained by a Gauss function due to the energy of laser beam are the Gaussian intensity, resulting in a Gaussian shape cross section of PMMA microchannel. The cross section of the PMMA microchannel (Figures 3.16, 3.17) depends on diode laser power, speed of X-Y movement and the thermal diffusion of PMMA. The effect of diode laser power and speed of X-Y movement were investigated on channel dimensions. Tables 3.15, 3.16 and Figure 3.18 were described the relationships between the speed of X-Y movement and the channel dimensions. The laser power was fixed at 5 W, whereas the speed of X-Y movement was varied from 1.0 to 10.0 mm s^{-1}. It was shown that the microchannels widths decreased with the speed of X-Y movement from 300 µm to 147 µm. In the case of microchannel depth, it dropped from 424 µm to 74 µm. Tables 3.17, 3.18 and Figure 3.19 shows the relationships between the diode laser power and the channel dimensions. The speed of X-Y movement was kept at a constant value of 4.0 mm s-1, whereas the diode laser power was varied from 2.5 W to 5.0 W. It was found that the width of the grooves went up from 193 µm to 393 µm with the increase in diode laser

ลิขสิทธิ์มหาวิทยาลัยเชียงใหม่
Copyright© by Chiang Mai University
All rights reserved

power, whereas the depth of microchannels increased significantly from 114 µm to 554 µm when the power laser was climbed. The results indicated that the depths and the widths of microchannel were opposite proportionate to the speed of X-Y movement. Due to the fact that when the speed of X-Y movement was very high, it exposed shorter time at each point and subsequently a little heat was absorbed by the PMMA substrate, leading to a good microchannel with the more shallow and narrow shape. The suitable dimensions of PMMA microchannel from diode laser mini-CNC machine was the width of 226 µm and the depth of 202 µm that used the diode laser power at 5 W and the scanning of X-Y movement of 3 mm s^{-1}. Since these sizes were close to geometric shape that allows the best form of dispersion zone in flow system to be obtained.

Table 3.15 The width of microchannel at constant laser power of 5 W

X-Y Speed (mm s^{-1})	**The width (µm)**			$\bar{x}$	**SD**
	1	**2**	**3**		
1	304	297	298	300	3.09
2	250	256	259	255	3.74
3	224	222	231	226	3.86
4	212	214	215	214	1.25
5	188	189	190	189	0.82
6	176	177	174	176	1.25
7	163	162	166	164	1.70
8	156	155	156	156	0.47
9	150	152	153	152	1.25
10	148	147	147	147	0.47

ลิขสิทธิ์มหาวิทยาลัยเชียงใหม่
Copyright© by Chiang Mai University
All rights reserved

Table 3.16 The depth of microchannel at constant laser power of 5 W

X-Y Speed (mm s^{-1})	The depth (μm)			$\bar{x}$	SD
	1	2	3		
1	425	420	426	424	2.62
2	370	372	368	370	1.63
3	202	198	205	202	2.87
4	132	136	142	137	4.11
5	130	125	127	127	2.05
6	103	108	100	104	3.30
7	95	96	96	96	0.47
8	89	91	92	91	1.25
9	81	74	84	80	4.19
10	71	75	76	74	2.16

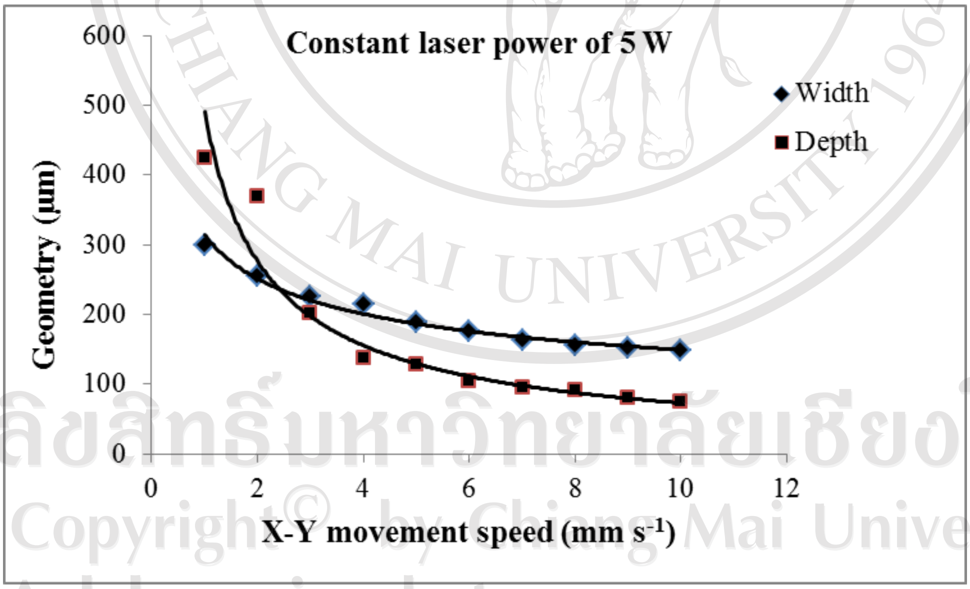

ลิขสิทธิ์มหาวิทยาลัยเชียงใหม่
Copyright© by Chiang Mai University
All rights reserved

Figure 3.18 Relationship between X-Y movement speed and geometric parameters

Table 3.17 The width of microchannel at constant X-Y movement speed of 4 mm s^{-1}

Laser power (W)	**The width (μm)**			$\bar{x}$	**SD**
	1	**2**	**3**		
2.5	193	190	195	193	2.05
3.0	204	203	200	202	1.70
3.5	222	225	230	226	3.30
4.0	265	262	265	264	1.41
4.5	329	333	330	331	1.70
5.0	349	355	354	353	2.62

Table 3.18 The depth of microchannel at constant X-Y movement speed of 4 mm s^{-1}

Laser power (W)	**The depth (μm)**			$\bar{x}$	**SD**
	1	**2**	**3**		
2.5	113	113	115	114	0.94
3.0	225	230	235	230	4.08
3.5	275	266	263	268	5.10
4.0	362	373	373	369	5.19
4.5	420	430	425	425	4.08
5.0	550	555	558	554	3.30

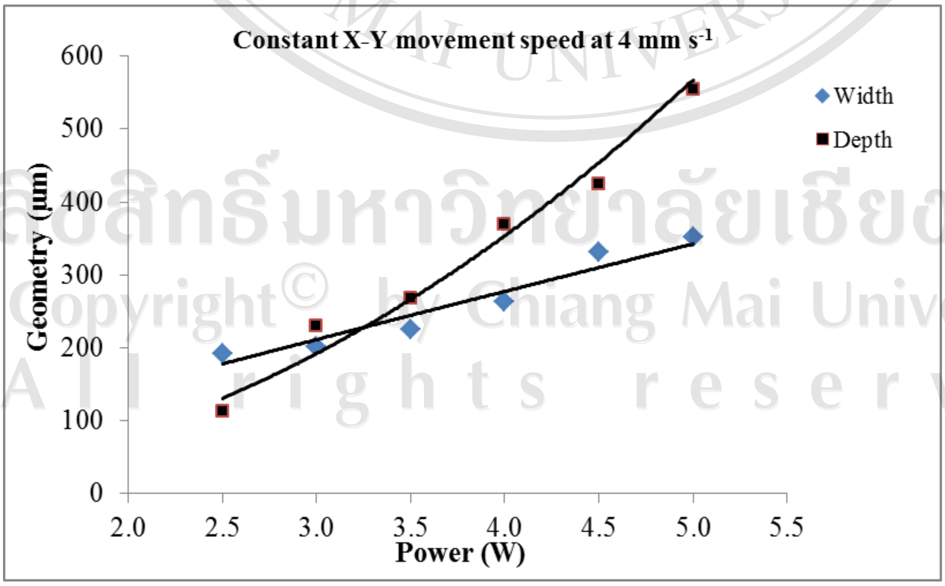

Figure 3.19 Relationship between laser power and geometric parameters

ลิขสิทธิ์มหาวิทยาลัยเชียงใหม่
Copyright© by Chiang Mai University
All rights reserved

3.2.4 The smoothness of microchannels

The smoothness of microchannels surface can minimize light scattering and leading to enhance the signal to noise ratio when the chip is applied to optical detection. In addition, the smoothness of surface can diminish the surface adsorption that can cause contamination in line and resulting band broadening of the signal. The smoothness of channel was studied by varying the speed of X-Y movement ranging between 4.0-10 mm s^{-1} and fixed the diode laser power at 5 W. The smoothness of PMMA channel was examined by SEM image. The results (Figure 3.20) displayed that the higher the speed, the rougher surface would be obtained. Therefore, the lower speed gives the smoother tiny channel surface.

It was obvious that the smoothness of microchannel surface could be improved by solvent exposure especially organic solvents which could be examined using SEM. To reduce surface roughness of PMMA tiny channel dichloromethane (CH_2Cl_2) was tested as organic solvent. After exposure to CH_2Cl_2 the surface of microchannels on the PMMA were examined by SEM and the SEM image (Figure 3.20) were observed. It can clearly be seen after CH_2Cl_2 vapor exposure, the surface was smoother when compare between before and after exposure to CH_2Cl_2. This method provides a low-cost, rapid and simple for surface smoothing.

ลิขสิทธิ์มหาวิทยาลัยเชียงใหม่
Copyright© by Chiang Mai University
All rights reserved

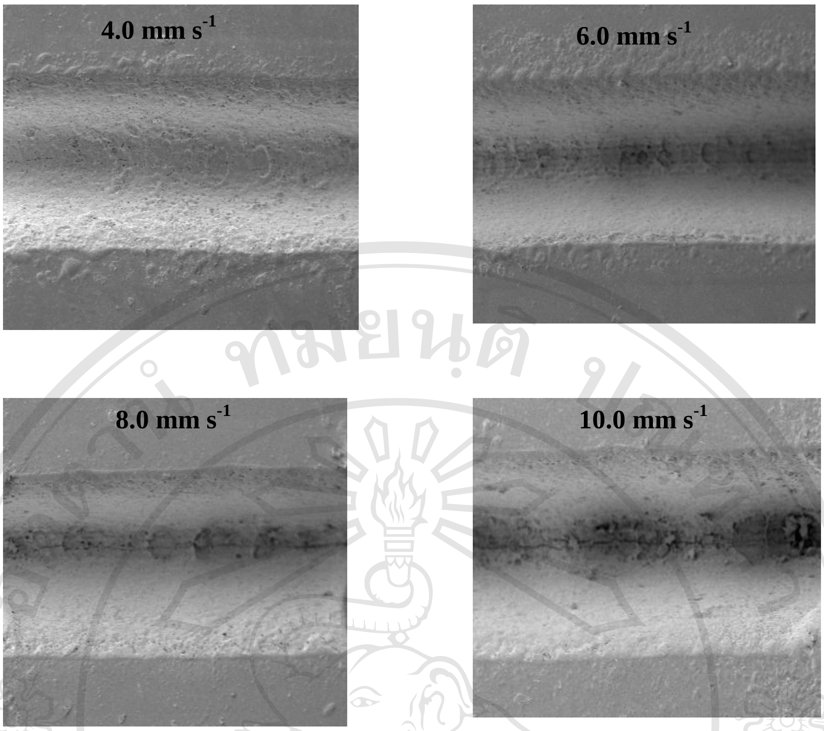

Figure 3.20 SEM images of PMMA substrates show the smooth of channel with different scanning speed (5 W laser power)

ลิขสิทธิ์มหาวิทยาลัยเชียงใหม่
Copyright© by Chiang Mai University
All rights reserved

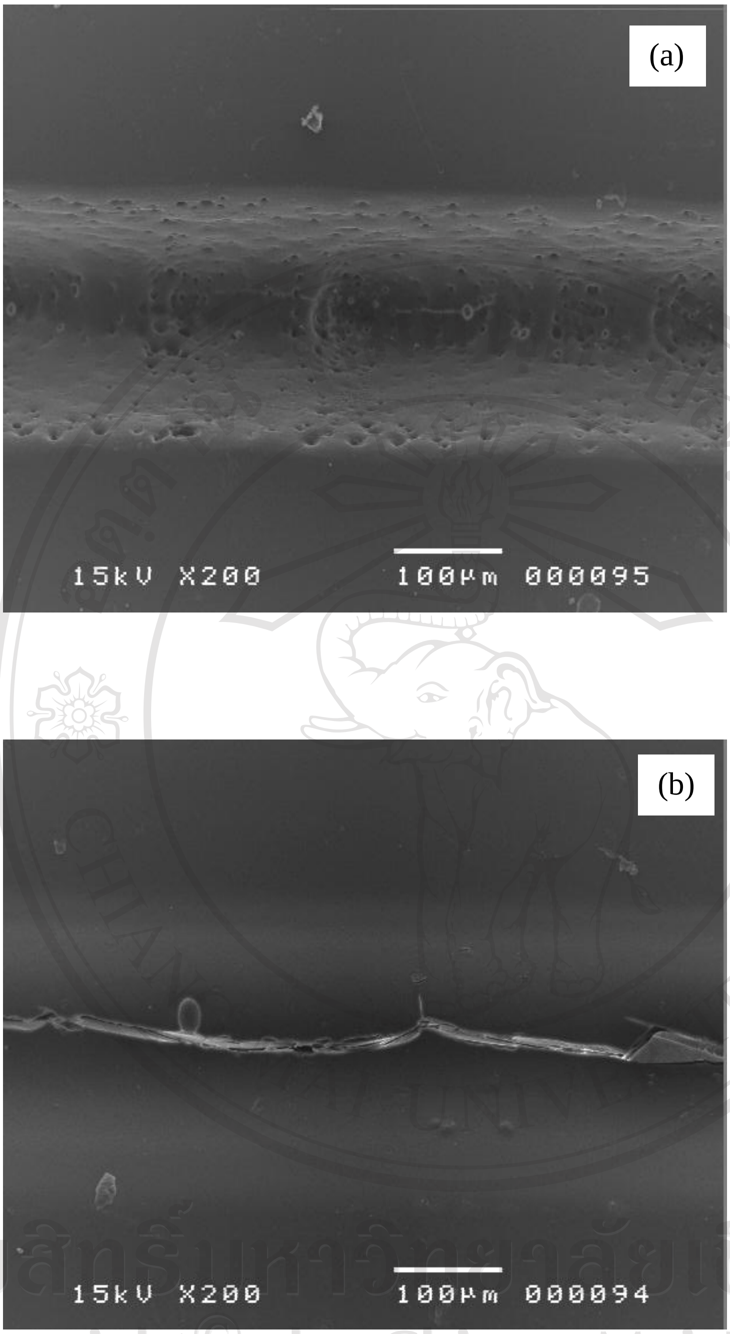

ลิขสิทธิ์มหาวิทยาลัยเชียงใหม่
Copyright© by Chiang Mai University
All rights reserved

Figure 3.21 SEM images of PMMA microchannel demonstrating the smooth effect of expose to CH_2Cl_2 solution; (a) before exposure to CH_2Cl_2 and (b) after exposure to CH_2Cl_2 for 10 min

3.2.5 Bonding of PMMA microchannels

The sealing of the open PMMA microchannels are essential step for making a chip. In this work, PMMA microchannels were sealed using thermal technique by polymerization on the surface between PMMA microchannel plates and blank PMMA plate. After two PMMA plates are exposed to heat, they start to soften at Tg (about 105ºC) and then many bonds are broken during bonding at a higher temperature (140ºC) and rejoined after cooling at room temperature. In summary, higher temperature and low pressure can proffer better bonding of PMMA, but bubble may be generated between two PMMA surfaces at too high temperature. Moreover, very high temperature can damage the structure of PMMA resulting loss of microchannel dimensions. SEM image (Figure 3.22) displays the cross section of bonded PMMA microchannel. It was found that the bonding interface almost no signs were saw. Due to the high bonding temperature that makes the dimensions of microchannel kept the Guassian shapes. The results display that the thermal bonding method is successful to make a well-defined microchannels PMMA chip. Figure 3.23 displays the steps for creating a PMMA chip.

ลิขสิทธิ์มหาวิทยาลัยเชียงใหม่
Copyright © by Chiang Mai University
All rights reserved

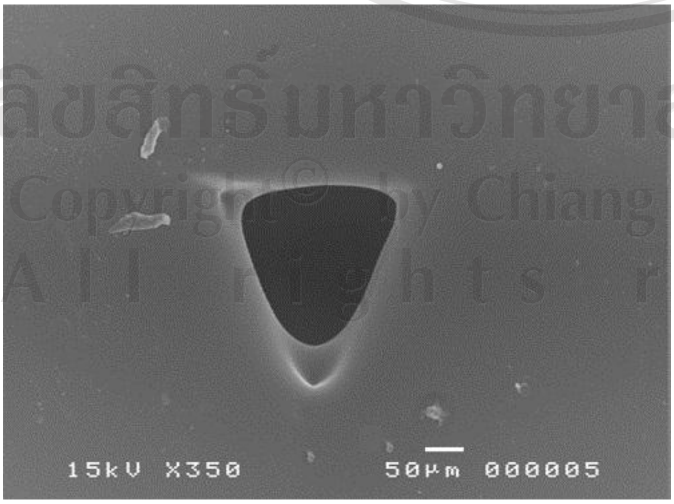

Figure 3.22 Cross section of the bonded microchannel

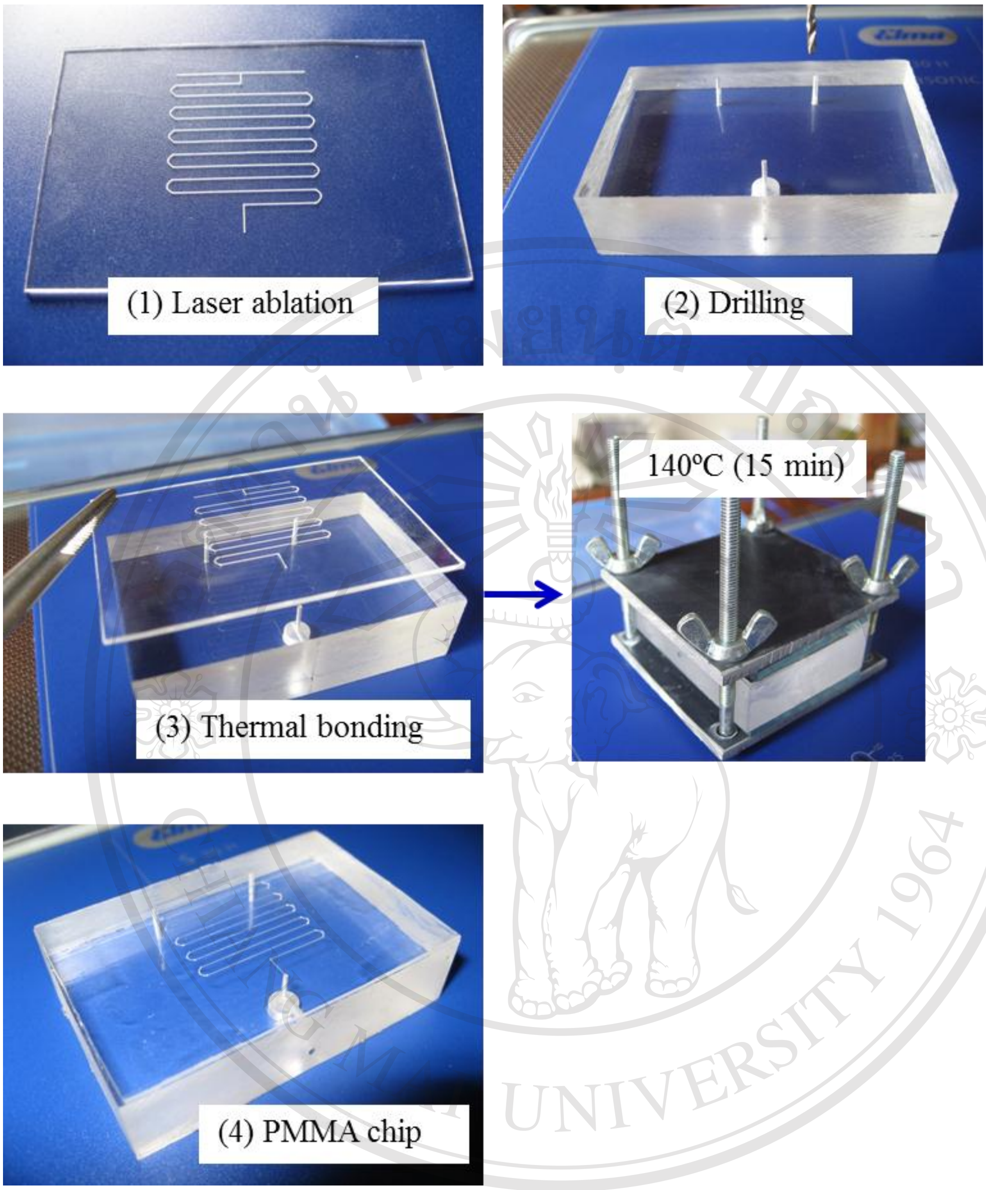

Figure 3.23 Fabrication procedures for the PMMA chip

ลิขสิทธิ์มหาวิทยาลัยเชียงใหม่
Copyright© by Chiang Mai University
All rights reserved

3.2.6 Validation of the proposed PMMA chip from diode laser technique

The developed automation microflow analyzer with PMMA chip has been tested to the determination of iron based on the complexation between iron (III) and chlortetracycline (CTC) resulting in an intense yellow water soluble product with an absorption maximum at 440 nm. It based on injection of CTC solution into the appropriate concentration of Fe(III) stream or water samples to µrFA system (Figure 2.8). The complex of sample (iron) and reagent (CTC) zone in T-junction microchannel (20 cm length) is then propelled towards the detection cell fixed at the end of the PMMA chip at appropriate flow rate. The yellow complex Fe(II)-$(CTC)_2$ is detected with spectrophotometry at 440 nm using USB4000 spectrometer. Calibration curve is achieved by plotting the increase in peak heights against several concentration of Fe(III). **This work was focus in the development of mini-CNC modified with diode laser for fabrication of PMMA chips, investigated parameters of adapted machine and selected the reaction of Fe(III)-CTC for tested the chip system**.

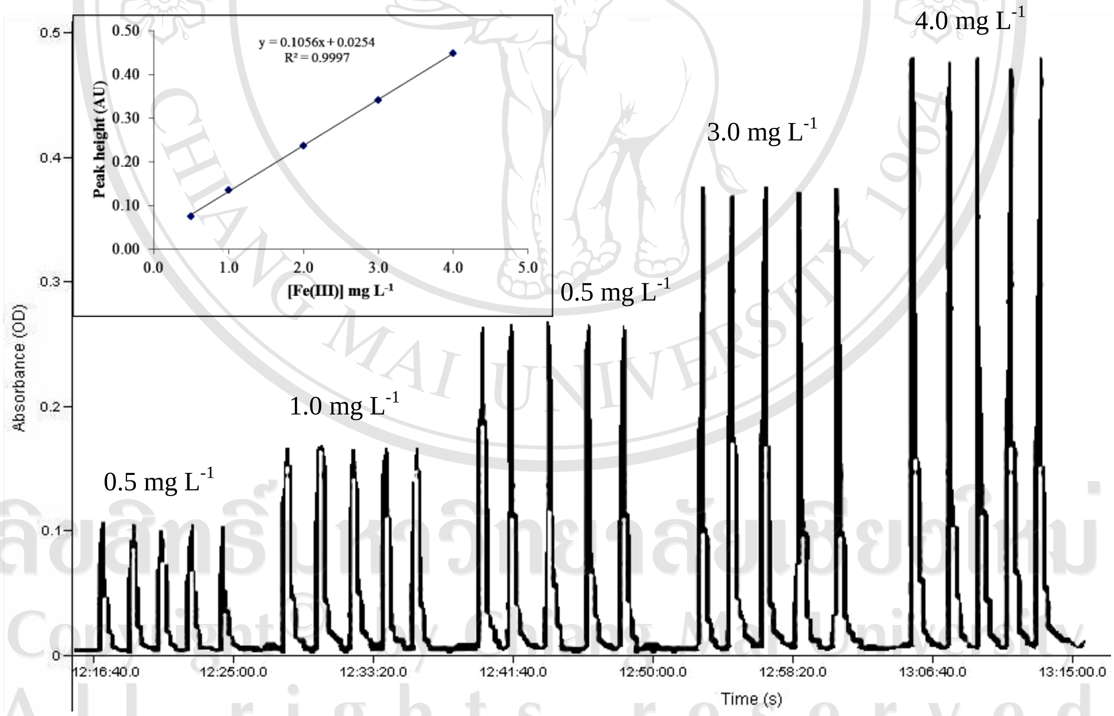

Figure 3.24 Calibration curve of standard Fe(III) solution

A linear range of calibration graph over the 0.5-4.0 mg L^{-1} Fe(III) was proved (Figure 3.24) with the regression equation achieved by plotting x (mg L^{-1} Fe(III)) versus y

ลิขสิทธิ์มหาวิทยาลัยเชียงใหม่
Copyright© by Chiang Mai University
All rights reserved

(peak height in AU) y = 0.1056x + 0.0254 (r^2=0.9997). Figure 3.24 demonstrates an example of the µrFA gram from PMMA chip.

3.2.7 Repeatability and reproducibility

The repeatability of the proposed method was determined by carrying out 11 replicate measurements of solutions containing 1.0 mg L^{-1} Fe(III) and the relative standard deviation was displayed to be 0.97%. The results were summarized in the Table 3.19. Moreover, the reproducibility of 11 replicate injections of the standard Fe(III) 2.0 mg L^{-1} solution was found to be 1.14%.

Table 3.19 Repeatability and reproducibility of replicate determination of Fe(III)

Experiment Number	**Peak height (AU)**	
	Repeatability	**Reproducibility**
1	0.137	0.235
2	0.135	0.242
3	0.137	0.240
4	0.134	0.237
5	0.136	0.241
6	0.134	0.235
7	0.135	0.238
8	0.136	0.237
9	0.137	0.242
10	0.136	0.239
11	0.138	0.235
$\bar{x}$	0.136	0.238
SD	0.0013	0.0027
RSD (%)	0.97	1.14

ลิขสิทธิ์มหาวิทยาลัยเชียงใหม่
Copyright © by Chiang Mai University
All rights reserved

3.2.8 Accuracy and sample throughput

The accuracy expressed in term of percentage recovery was verified by spiking various concentration of Fe(III) standard solution into the water samples. The recoveries of the added Fe(III) were found to over the range of 101 - 105% (see appendix D) indicating that the recommended procedure was accurate. In addition, the developed method was rapid with an average t_{base} of 90 s (n=7) together with the sample throughput for the proposed method was found to be 40 samples h^{-1}.

3.2.9 Application to water samples analysis

The proposed µrFA system was displayed to be appropriate for measurements with a detection limit of 0.17 mg L^{-1}. The proposed method was acceptably applied to the determination of iron(III) in water samples. The water samples from Chiang Mai University, Ping River and canal in Chiang Mai Province were collected in 2000 mL polyethylene bottles without acidified by concentrated nitric acid and analysed instantly after digestion. Results were displayed in Table 3.20. Comparative results obtained by both the proposed µrFA and FAAS methods were in good agreement verified by the student t-test. The calculated value of *t* for Fe(III) assay are less than the theoretical value (4.30) for two degrees of freedom signifying that results obtained by both methods display no significant difference at 95% confidence intervals.

ลิขสิทธิ์มหาวิทยาลัยเชียงใหม่
Copyright© by Chiang Mai University
All rights reserved

Table 3.20 Comparative determination of Fe(III) in water samples by the proposed µrFA and FAAS methods

Water sample	Fe(III) content (mg L^{-1})		$t_{calculated}$
	µFA method*	**FAAS method***	
Ang-Keaw	1.695 ± 0.021	1.743	-3.235
Ang-Karset	1.787 ± 0.031	1.727	3.064
Tap water	1.925 ± 0.035	1.852	3.645
Ping River	0.988 ± 0.006	1.001	-3.640
Chon Pra Than Canal	0.926 ± 0.005	0.932	-2.078

* mean of triplicate

In summary, the mini-CNC machine modified with diode laser has a powerful for fabrication of a PMMA chip. This machine is far cheaper than a commercial machine and need small area for operation. Moreover, the proposed µFA analyzer with PMMA chip has proven to be promising as a forceful analytical device for metal ion determinations in real samples. In addition, the µrFA system, employed small reagent volume and generated chemical waste less than 4 mL h^{-1}. The proposed PMMA chip with microdevice system related to a green analytical technique with very small reagent consumption, very small chemical waste generation, small instrument and portable device that can be applied for on-site monitoring. These applications of µrFA have been studied in optimized conditions and analytical characteristics that were described in appendix D.

ลิขสิทธิ์มหาวิทยาลัยเชียงใหม่
Copyright © by Chiang Mai University
All rights reserved

3.3 Fabrication of PMMA chip with CO_2 laser for determination of zinc by microflow analysis using xylenol orange as complexing agent

In this section, a greener analytical method based on lab-on-a-chip using a micro reactor fabricated by CO2 laser to create microchannels on PMMA coupled with μFA system. The μFA analyzer was tested for Zn(II) determination with spectrophotometric detection. More details will be discussed as follows:

3.3.1 The patterns of PMMA chip

All patterns of PMMA chip were designed using drawing software (Figure 3.25) and the complete PMMA microchannels from CO_2 laser machine followed the design (Figure 3.26). Y-junction patterns are one micro reactor with two inlet holes and one outlet hole of PMMA chip (Figure 3.25 a, b, c) with the length of microchannel as 10, 20 and 30 cm respectively. Next, two micro reactor with three inlet and one outlet reservoirs; (Figure 3.25 d, e, f, g, h, i) with the length of microchannels are 20, 30, 40, 40, 50 and 60 cm respectively. In addition, the spiral shape can create with the microchannel length of 40 cm (Figure 3.25 j). The area of U-turns channel can be applied for heat transfer, polymer chain reaction and chemical reaction. The complexity of the pattern can be designed and modified easily using common drawing software in less than an hour. Each pattern can be generated in two min. Time for fabrication depends on the pattern and the length of microchannel, longer channels take more time for creation.

ลิขสิทธิ์มหาวิทยาลัยเชียงใหม่
Copyright© by Chiang Mai University
All rights reserved

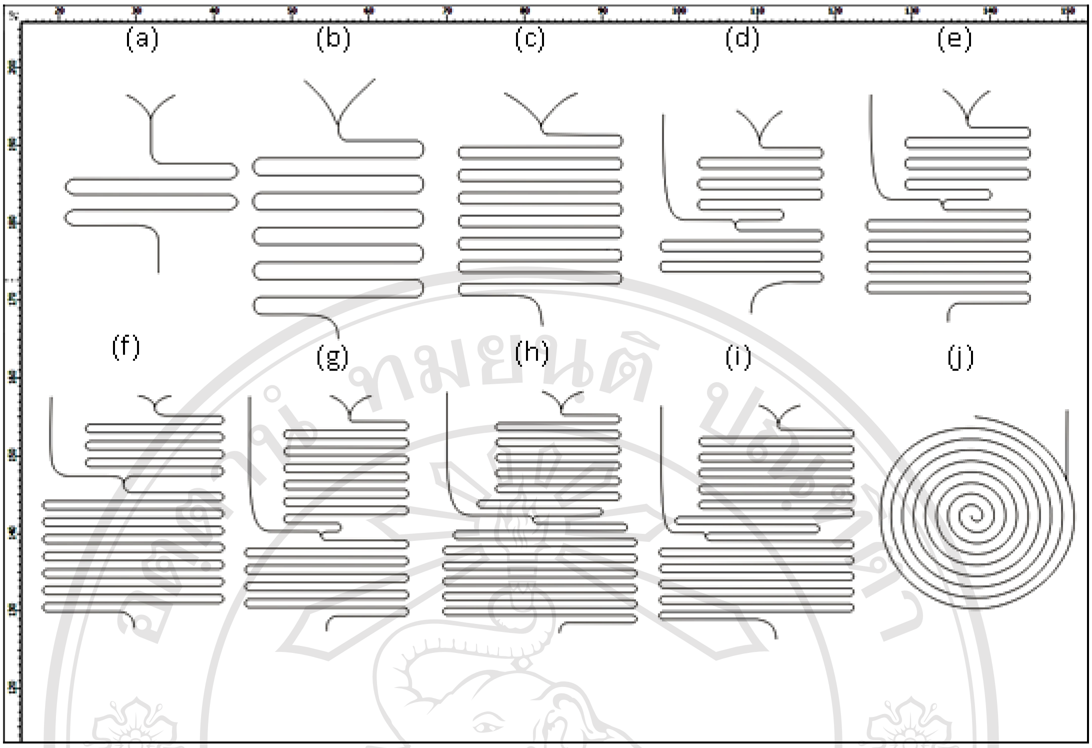

Figure 3.25 Y-junction patterns of PMMA microchannels

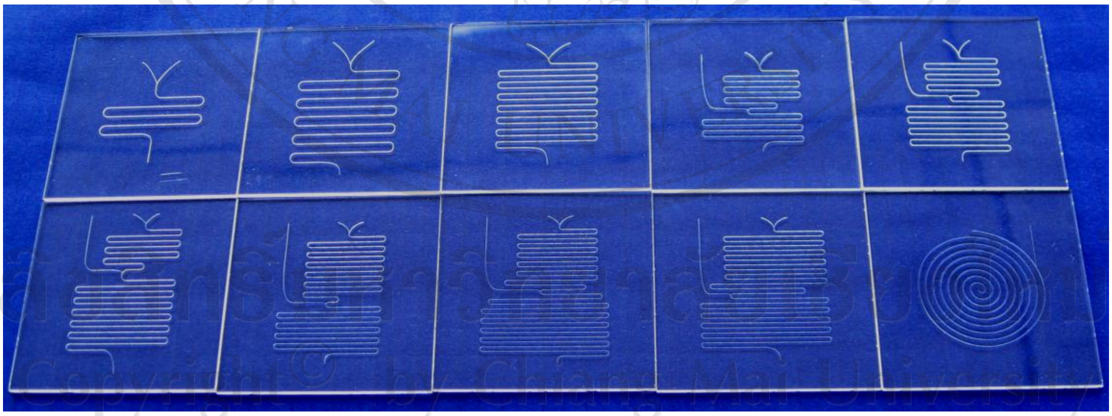

Copyright© by Chiang Mai University
All rights reserved

Figure 3.26 The complete PMMA microchannel from CO_2 laser machine

The CO_2 laser discharges radiation beam continuously with a relatively long specific wavelength of 1060 nm. It is available with a wide range of scanning speed and laser power at suitable price of instrument. When the focused laser beam exposes the PMMA surface, the PMMA is first melted as a spot on the surface then decomposed and vaporized leading to a blank channel on the PMMA, while most of the melted PMMA is re-solidified in the excited laser beam. By this mean the moving laser beam with enough power is able to cut PMMA sheet such as microchannels and holes in a polymer. Figure 3.27 displayed the cross section of PMMA microchannel from CO_2 laser. The energy of CO_2 laser is a Gaussian format, leading to a Gaussian shaped PMMA microchannels.

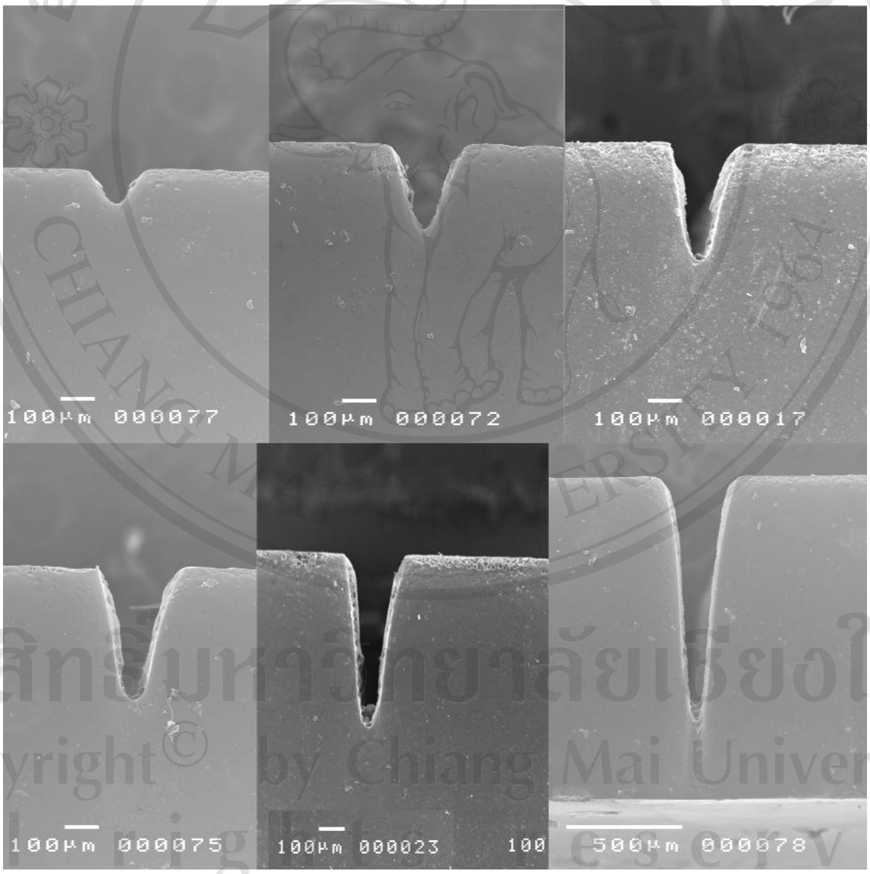

Figure 3.27 Cross section of the PMMA microchannel

ลิขสิทธิ์มหาวิทยาลัยเชียงใหม่
Copyright© by Chiang Mai University
All rights reserved

3.3.2 The depth and the width of microchannel PMMA using CO_2 laser

The depth and the width of microchannels on the PMMA are studied by SEM as cross sections through microchannels. The cross section of microchannels depends on the scanning beam speed, laser power and the thermal diffusion of PMMA sheet. The influence of the laser power and scanning beam speed of CO_2 laser was inspected. Tables 3.21, 3.22 and Figure 3.28 described the relationships between the beam speed and the channel dimensions. The laser power was fixed at 8 W, whereas the beam speed of CO_2 laser was varied from 1 to 20 mm s^{-1}. It was demonstrated that the microchannels widths decreased from 249 µm to 112 µm with increasing the scanning of laser beam. In the case of microchannel depth, it dropped from 528 µm to 26 µm. Moreover, Tables 3.23, 3.24 and Figure 3.29 show the relationships between the diode laser power and the channel dimensions. The speed of laser beam was kept at a constant value of 5.0 mm s^{-1}, whereas the diode laser power was varied from 8 W to 16 W. It was displayed that the width of the grooves went up from 195 µm to 418 µm with the increase in CO_2 laser power, whereas the depth of microchannels increased significantly from 194 µm to 890 µm when the laser power was climbed. The results indicate that the depths and the widths of microchannel were opposite proportionate to the scanning beam speed. Due to the fact that when the beam speed is very high, it exposes shorter time at each point and consequently less heat is absorbed by the PMMA substrate, leading to a good microchannel with the shallower and narrower configuration. The geometric dimensions of PMMA microchannel produces by the CO_2 laser machine is 193 µm in width and the depth of 194 µm that use the CO_2 laser power at 8 W and the scanning beam of 3 mm s^{-1}. Due to these sizes are close to the geometric shape leading to the best form of dispersion zone in the flow system. However, trends of microfluidic device need less chemical solution flowing in the chip, sometime

ลิขสิทธิ์มหาวิทยาลัยเชียงใหม่
Copyright© by Chiang Mai University
All rights reserved

the symmetrical dimensions of microchanels of the chip are not regarded. Generally, the proper dimension of PMMA chip is over the range of 50-200 μm of width and depth.

Table 3.21 The width of microchannel at constant laser power of 8 W

Beam Speed (mm s^{-1})	**The width (μm)**			**$\bar{x}$**	**SD**
	1	**2**	**3**		
1	247	249	250	249	1.25
2	235	239	240	238	2.16
3	227	228	230	228	1.25
4	210	210	212	211	0.94
5	191	193	196	193	2.05
6	183	184	182	183	0.82
7	174	175	173	174	0.82
8	169	167	166	167	1.25
9	164	163	160	162	1.70
10	155	157	155	156	0.94
11	150	151	148	150	1.25
12	146	145	143	145	1.25
13	141	140	138	140	1.25
14	136	135	132	134	1.70
15	129	131	128	129	1.25
16	127	128	125	127	1.25
17	124	122	120	122	1.63
18	119	117	118	118	0.82
19	117	116	115	116	0.82
20	111	113	113	112	0.94

ลิขสิทธิ์มหาวิทยาลัยเชียงใหม่
Copyright© by Chiang Mai University
All rights reserved

Table 3.22 The depth of microchannel at constant laser power of 8 W

Beam Speed (mm s^{-1})	**The depth (µm)**			**$\bar{x}$**	**SD**
	1	**2**	**3**		
1	525	531	528	528	2.45
2	340	342	345	342	2.05
3	268	278	270	272	4.32
4	227	220	225	224	2.94
5	193	194	196	194	1.25
6	165	176	168	170	4.64
7	154	156	159	156	2.05
8	130	125	132	129	2.94
9	121	123	119	121	1.63
10	106	105	108	106	1.25
11	94	97	96	96	1.25
12	88	84	86	86	1.63
13	82	80	83	82	1.25
14	77	75	74	75	1.25
15	63	62	60	62	1.25
16	51	55	53	53	1.63
17	45	45	44	45	0.47
18	38	37	39	38	0.82
19	32	30	33	32	1.25
20	27	27	25	26	0.94

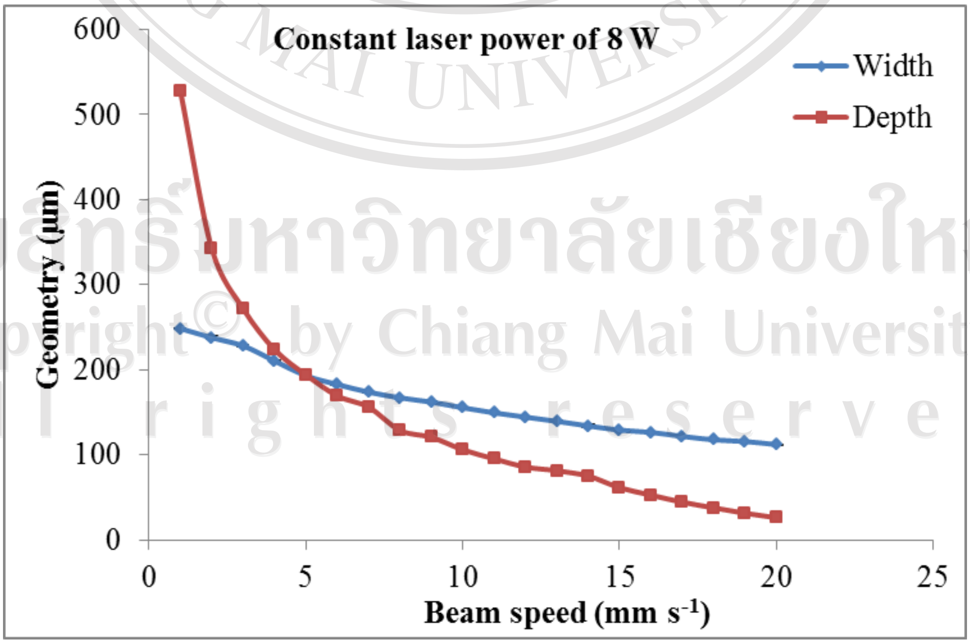

Figure 3.28 Relation of beam speed on geometric parameters

ลิขสิทธิ์มหาวิทยาลัยเชียงใหม่
Copyright© by Chiang Mai University
All rights reserved

Table 3.23 The width of microchannel at constant beam speed of 5 mm s^{-1}

Laser power (W)	The width (µm)			$\bar{x}$	SD
	1	2	3		
8.0	195	192	197	195	2.05
8.8	235	231	235	234	1.89
9.6	255	256	258	256	1.25
10.4	278	275	272	275	2.45
11.2	302	305	307	305	2.05
12.0	335	338	340	338	2.05
12.8	361	364	366	364	2.05
13.6	385	384	382	384	1.25
14.4	391	392	389	391	1.25
15.2	401	405	408	405	2.87
16.0	415	418	420	418	2.05

Table 3.24 The depth of microchannel at constant beam speed of 5 mm s^{-1}

Laser power (W)	The depth (µm)			$\bar{x}$	SD
	1	2	3		
8.0	193	196	194	194	1.25
8.8	236	238	243	239	2.94
9.6	289	296	298	294	3.86
10.4	350	342	348	347	3.40
11.2	472	477	479	476	2.94
12.0	535	542	539	539	2.87
12.8	665	670	671	669	2.62
13.6	750	755	760	755	4.08
14.4	814	817	820	817	2.45
15.2	860	866	864	863	2.49
16.0	888	897	886	890	4.78

ลิขสิทธิ์มหาวิทยาลัยเชียงใหม่
Copyright© by Chiang Mai University
All rights reserved

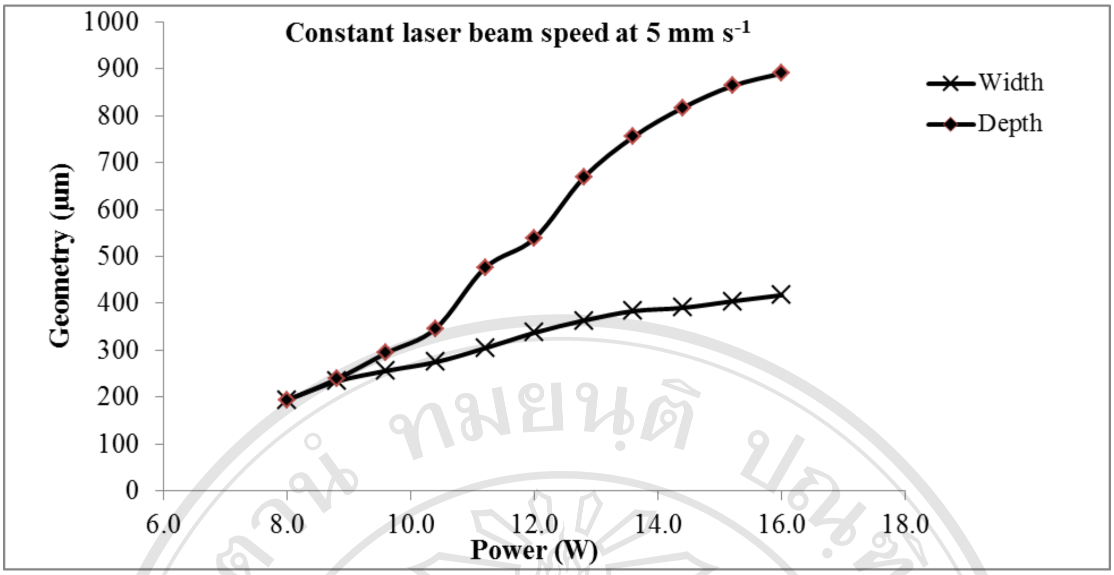

Figure 3.29 Relation of laser power on geometric parameters

3.3.3 The smoothness of PMMA microchannels

The smoothness of channel walls was studied by varied the speed of laser beam over the range of 4.0-10 mm s^{-1} and fixed the CO_2 laser power at 8 W. The smoothness of PMMA channel was examined by SEM image. SEM image can display a clear picture to describe the surface roughness. The results (Figure 3.30) displayed that the more increment of the speed leading to the increasing in the rough surface. Therefore, lower the speed gives rise to the smoother of tiny channel surface. The cause of roughness surface may be occur from the changed temperatures exposed to surface leading to PMMA experiences different status.

To reduce the PMMA surface roughness, the microchannels surface was improved by solvent exposure that was described earlier section 3.2.4.

ลิขสิทธิ์มหาวิทยาลัยเชียงใหม่
Copyright© by Chiang Mai University
All rights reserved

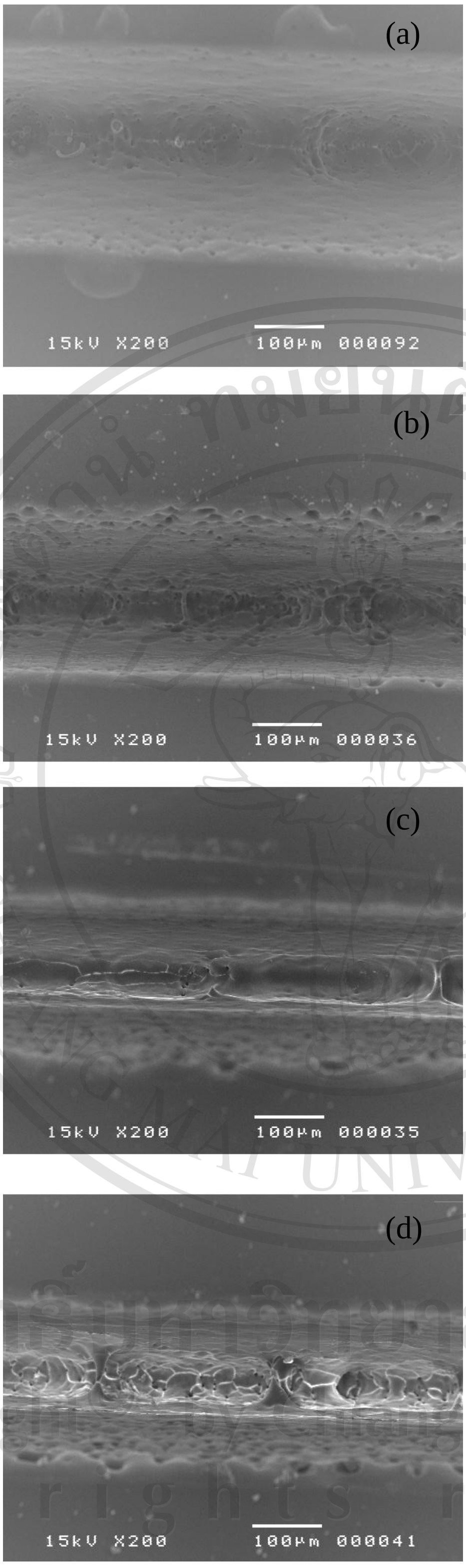

Figure 3.30 SEM images close up of PMMA microchannels with beam speed of 5 (a), 10 (b), 15 (c) and 20 (c) mm s^{-1} and fixed laser power of 8 W

ลิขสิทธิ์มหาวิทยาลัยเชียงใหม่
Copyright by Chiang Mai University
All rights reserved

3.3.4 Bonding of PMMA chip

The dimensions of PMMA microchannels were 194 µm wide and 195 µm deep that were selected for bonding. PMMA contains of the covalent bond between the methacrylate monomers molecules with serving as the backbone in the PMMA. SEM image (Figure 3.31) displays the cross section of bonded PMMA microchannel. It was shown that the bonding interface almost no signs were observed. Due to the high bonding temperature that makes the dimensions of microchannel to be the Guassian shapes. The results displayed that the thermal bonding method was successful to apply for making PMMA chip. Figure 3.32 shows the steps for fabrication of PMMA chip.

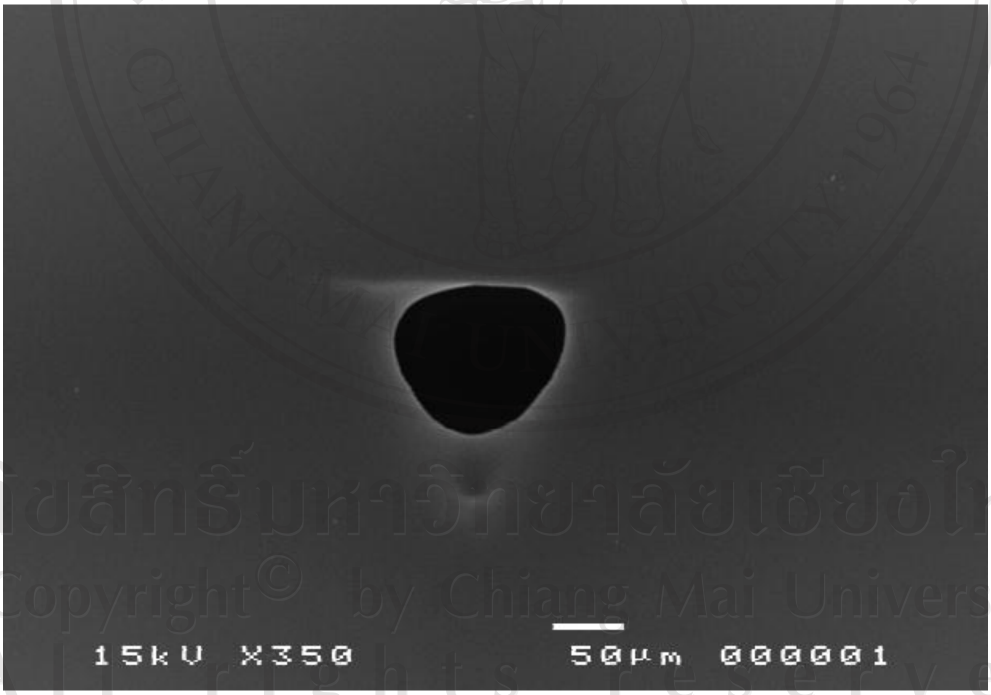

Figure 3.31 SEM image of a cross section of a bonded PMMA chip

ลิขสิทธิ์มหาวิทยาลัยเชียงใหม่
Copyright© by Chiang Mai University
All rights reserved

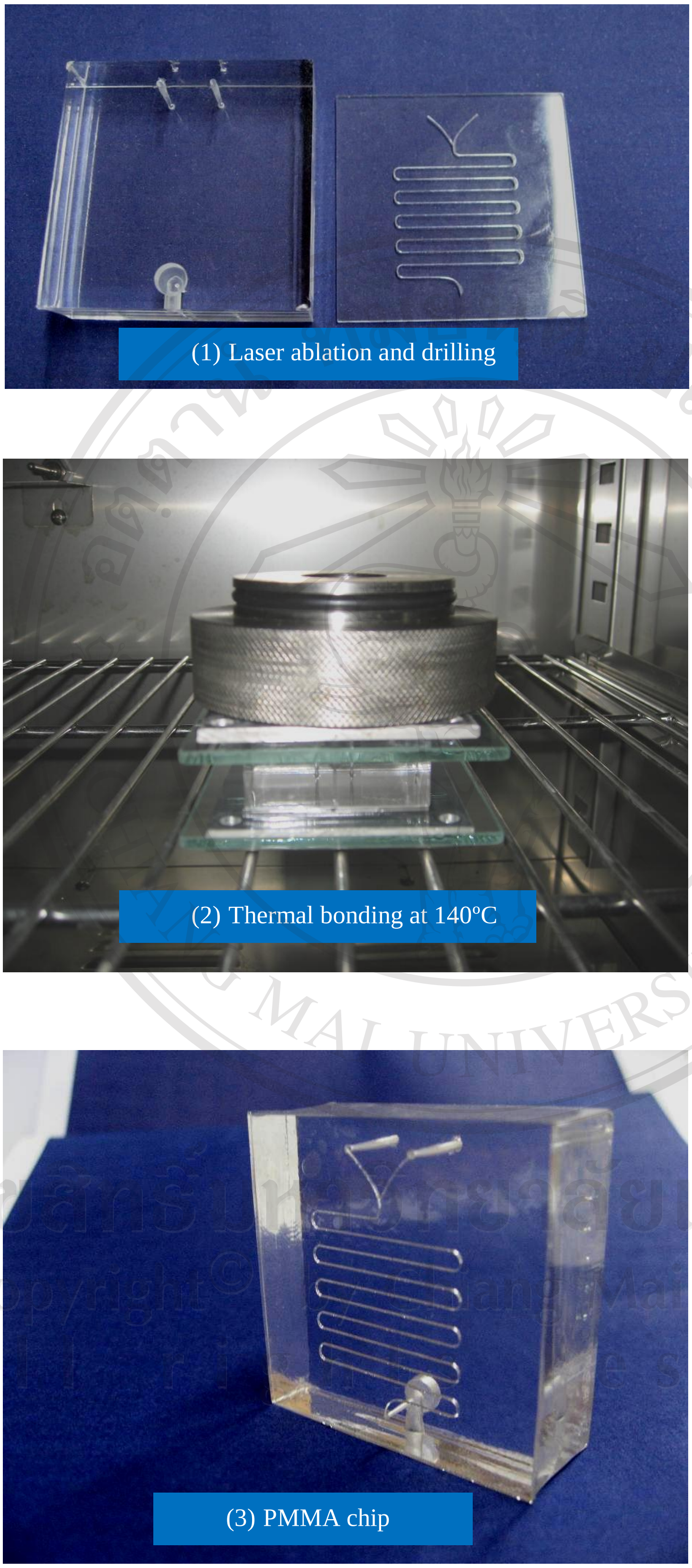

Figure 3.32 Summary the steps for fabrication PMMA chip (4.0 x 4.0 cm^2)

ลิขสิทธิ์มหาวิทยาลัยเชียงใหม่
Copyright© by Chiang Mai University
All rights reserved

3.3.5 Preliminary study on the absorption spectra of Zn(II)-xylenol orange complex in the presence of quinine photosensitizer

Zn(II) was examined using the reaction between Zn(II) and xylenol orange (XO) as previously studied by Benamor et al. [261] and Staden and Tlowana [262]. The structure formula of xylenol orange was shown in Figure 3.33. The absorption spectrum of the red-violet colored complex between Zn(II) ions and XO reaction in the absence and presence of quinine photosensitizer, along with their reagent blank over the range of 380–700 nm are scanned using Jenway 6400 Spectrophotometer. It was found that the absorption spectra of XO show at 432 nm with yellow color solution. When Zn(II) forms complex with XO, the color changes from yellow to red-violet is visually observed. The maximum absorbance of Zn(II)-XO complex occurs at 570 nm (Figure 3.34). The red-violet complex reduces the absorption of yellow XO at 432 nm, but it still appears due to the residual color of XO. The effect of quinine hydrochloride photosensitizer to Zn(II)-XO was studied. It was shown that quinine hydrochloride increased the absorption of complex significantly (Figure 3.34 (6), (7), (8)). Different concentration of Zn(II)-XO 1 ppm, 2 ppm and 3 ppm without and with quinine hydrochloride resulting the absorbance increase from 0.170 to 0.276 (Figure 3.34 (3), (6)), 0.376 to 0.526 (Figure 3.34 (4), (7)) and 0.494 to 0.723 (Figure 3.34 (5), (8)) respectively. Therefore, determination of Zn(II) using XO complexing agent was applied to PMMA chip by increasing the sensitivity with quinine hydrochloride.

ลิขสิทธิ์มหาวิทยาลัยเชียงใหม่
Copyright© by Chiang Mai University
All rights reserved

3.3.6 Determination of Zn(II) by micro flow analysis using xylenol orange as complexing agent

In this study, the method for Zn(II) determination by μFA using XO as chromogenic reagent is based on the measurement of absorbance increasing from

Zn(II))-XO complex with quinine hydrochloride as photosensitizer in an acetate buffer solution in the Y-junction microchannel on the PMMA microflow analyzer. The Zn(II)-XO complex was measured as absorbance at 590 nm**.** In this case the sensitivity of the complexation reaction between Zn(II) and XO should be improved prior to analysis by μFA system. Therefore, quinine hydrochloride was used as photosensitizer to enhance the absorbance arising from the Zn(II)-$(XO)_2$ complex. The stoichiometry of the Zn(II):XO was found to be 1:2 studied by mole ratio method [261, 262]. Therefore, in this investigation, an effort was made to develop a simple, selective, reproducible and sensitive microflow analyzer system with a PMMA chip for the determination of Zn(II) in water samples. Various conditions influencing the sensitivity of this proposed system such as the pH, concentration of XO solution, flow rate of the solutions, sample volume and concentration of quinine hydrochloride were optimized by employing the univariate method. This system was adopted as a basis to develop the selective and sensitive determination of Zn(II) at mg L^{-1} levels using the fabricated microflow system with spectrophotometric determination, which could be precise and accurate as well as those obtained using the conventional FIA manifold.

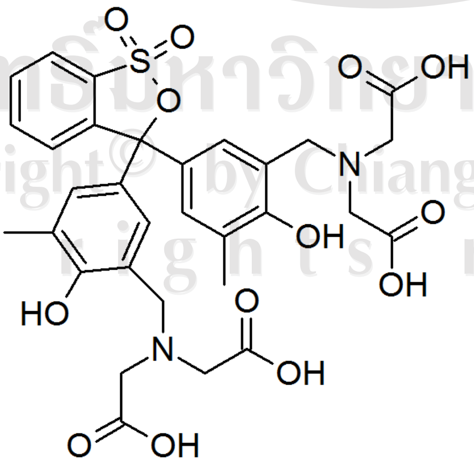

ลิขสิทธิ์มหาวิทยาลัยเชียงใหม่
Copyright© by Chiang Mai University
All rights reserved

Figure 3.33 The structure formula of xylenol orange [254]

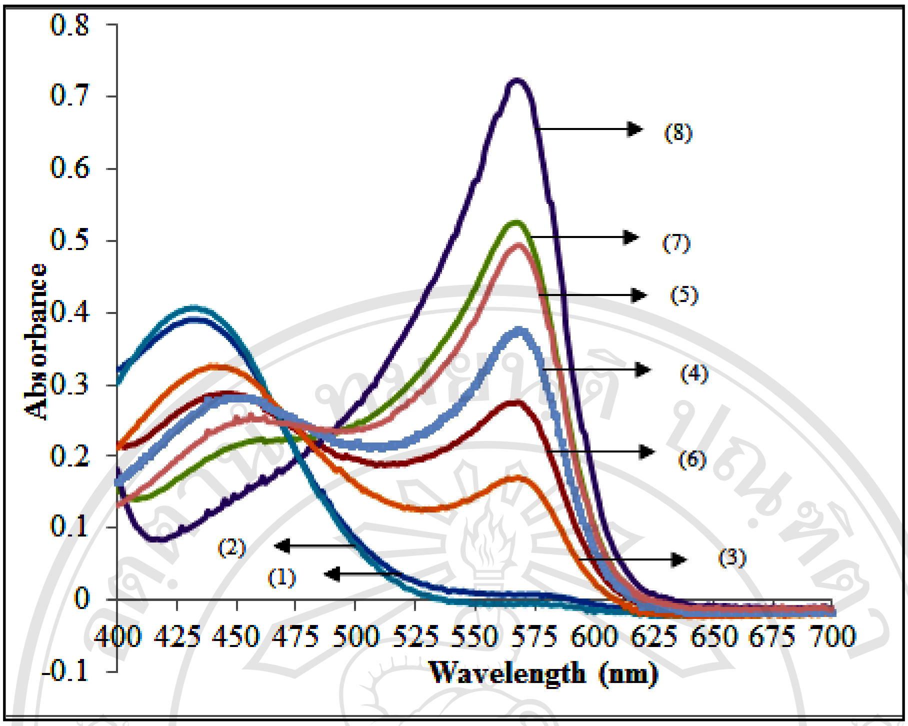

Figure 3.34 Absorption spectra of XO (1); XO-quinine (2); 1 ppm of Zn(II)-XO (3), 2 ppm of Zn(II)-XO (4), 3 ppm of Zn(II)-XO (5) against XO blank at pH 5.0; 1 ppm of Zn(II)-XO (6), 2 ppm of Zn(II)-XO (7), 3 ppm of Zn(II)-XO (8) against XO mixed with quinine blank at pH 5.0, XO concentration : 3.0 x 10^{-5} mol L^{-1}; quinine hydrochloride concentration : 2.0×10^{-3} mol L^{-1}

3.3.7 Design and fabrication of the micro flow system for zinc (II) determination

The PMMA chip system was specially designed with Y-junction and fabricated as a micro reactor used in the µFA manifold to miniaturize the conventional FIA manifold development of green analytical techniques which were environmentally friendly methods for analyzing real samples. The proposed µFA analyzer was tested for determining Zn(II). The system was said to be the green technique due to its reduction of sample and reagents consumption from several mL to µL or nL levels and small production of hazardous waste to human health and the

ลิขสิทธิ์มหาวิทยาลัยเชียงใหม่
Copyright© by Chiang Mai University
All rights reserved

environment. It is also portable device for on-site analysis because all functions of the system was miniaturized, which was superior to all traditional analytical techniques. The microflow reactor for Zn(II) determination was displayed in Figure 3.35. A Y-junction with micro coil U-turns channels on a PMMA chip was fabricated by means of the CO_2 laser machine that was described in previous section and connected with two flow lines. The first flow line was connected with a ten-port selection valves with zero dead volume (V) which was used for injecting small volume of sample or standard solution (S) into the buffered reagent stream. Another flow line was used for transporting the buffered reagent (R) into the PMMA chip device (C). The fabricated chip was covered with PMMA plate, where a small flow through cell (2μL) was positioned, which was connected with two fiber optic probes. The first one was placing at the end of flow cell in the PMMA plate which was connected to the USB4000 spectrophotometer (D). The second one was placing at the vertical axis under the PMMA chip which was connected to the light emitting diode (LED) white-light super bright as light source. Sample or standard solutions (S) was introduced with accurate volume into the system by time based injection using a ten-port selection valves with zero dead volume (V) controlled by using home-made SIA software. It is also used for controlling the micro peristaltic pump (P) with small pump tubing to transport the reagent at with appropriate flow rate (40 $\mu L\ min^{-1}$) flowing through the system. By this design, using the LED super bright instead of tungsten lamp is light source for the USB4000 spectrometer which provided higher reproducible signal with lower noise than the tungsten one. In addition, the absorbance is recorded with Spectrasuite Software. Figure 3.36 presented the intensity of light from the white LED that passed through the detection cell of the PMMA chip. It displayed the range of 450-750 nm wavelengths which was very useful for

ลิขสิทธิ์มหาวิทยาลัยเชียงใหม่
Copyright© by Chiang Mai University
All rights reserved

absorption detection of colored products. The proposed μFA system consumed less sample/reagent volume and released less waste than the traditional FI system.

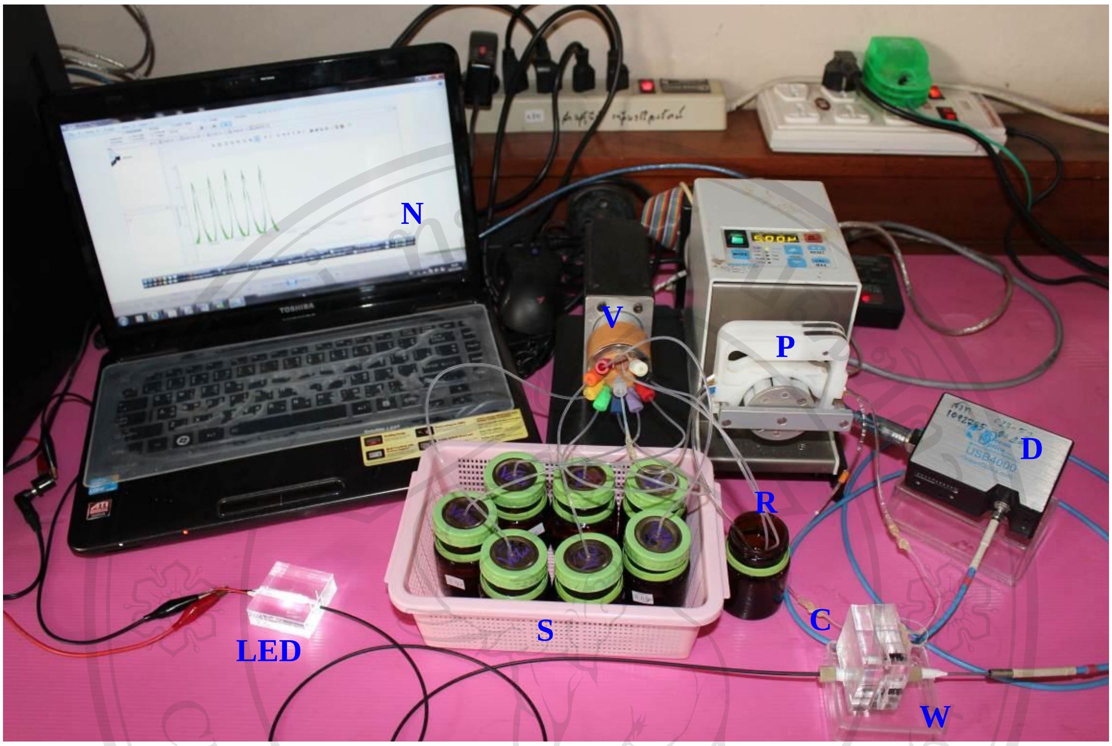

Figure 3.35 The microflow analyzer for Zn(II) determination: S, sample; R, buffered XO; V, selection valve (Valcol Instrument); P, pump; C, a PMMA chip; LED, light source; D, spectrophotometer (USB4000); N, computer; W, waste

ลิขสิทธิ์มหาวิทยาลัยเชียงใหม่
Copyright© by Chiang Mai University
All rights reserved

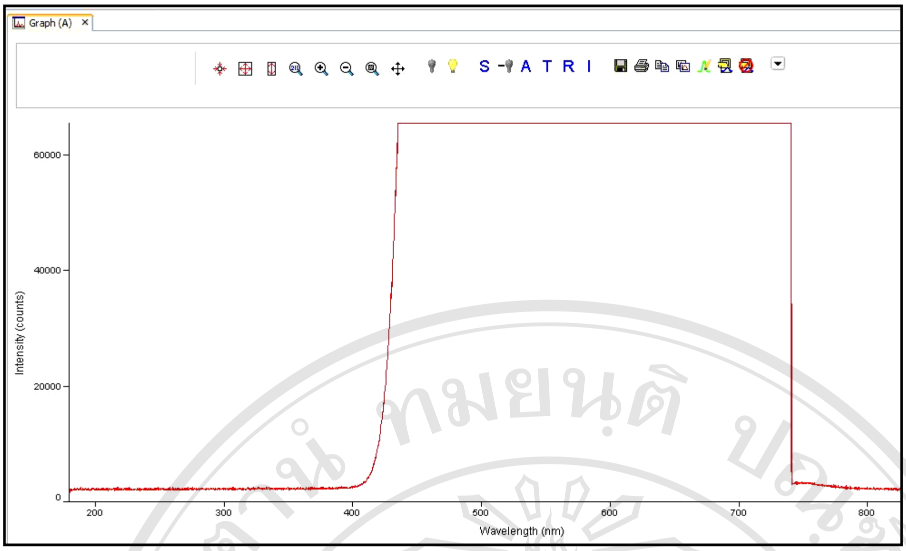

Figure 3.36 The intensity of light pass through the detection cell of PMMA chip

3.3.8 Optimization of the experimental conditions by univariate method

The optimum conditions for Zn(II) determination was done by a univariate method. The value of one variable was changed while keeping the other variables at their constant values. By maintaining that variables at its optimum value, another was studied. This analysis was intended at development of a novel μFA spectrophotometric method for determination of Zn(II) based on reaction with XO in the presence of quinine hydrochloride photosensitizer. In all experiments, five replicate measurements were accomplished for each studied parameter. All optimum values were chosen by consider from the maximum sensitivity, stability of the base line, low or no positive blank signals and low standard deviation. Preliminary conditions employed were as displayed in Table 3.25. The signal obtained from the proposed μFA system for Zn(II) determination as 1.0 ppm is shown in Figure 3.36. This method is suitable for the determination of Zn(II) in water samples.

ลิขสิทธิ์มหาวิทยาลัยเชียงใหม่
Copyright© by Chiang Mai University
All rights reserved

Table 3.25 Preliminary conditions before optimization of the PMMA μFA systems

Parameters	**Fixed value**
Wave length (nm)	580
pH	5.0
XO concentration (x 10^{-4} mol L^{-1})	1.0
Quinine hydrochloride concentration (x 10^{-4} mol L^{-1})	1.0
Injection volume (μL)	5
Flow rate (μL min^{-1})	40

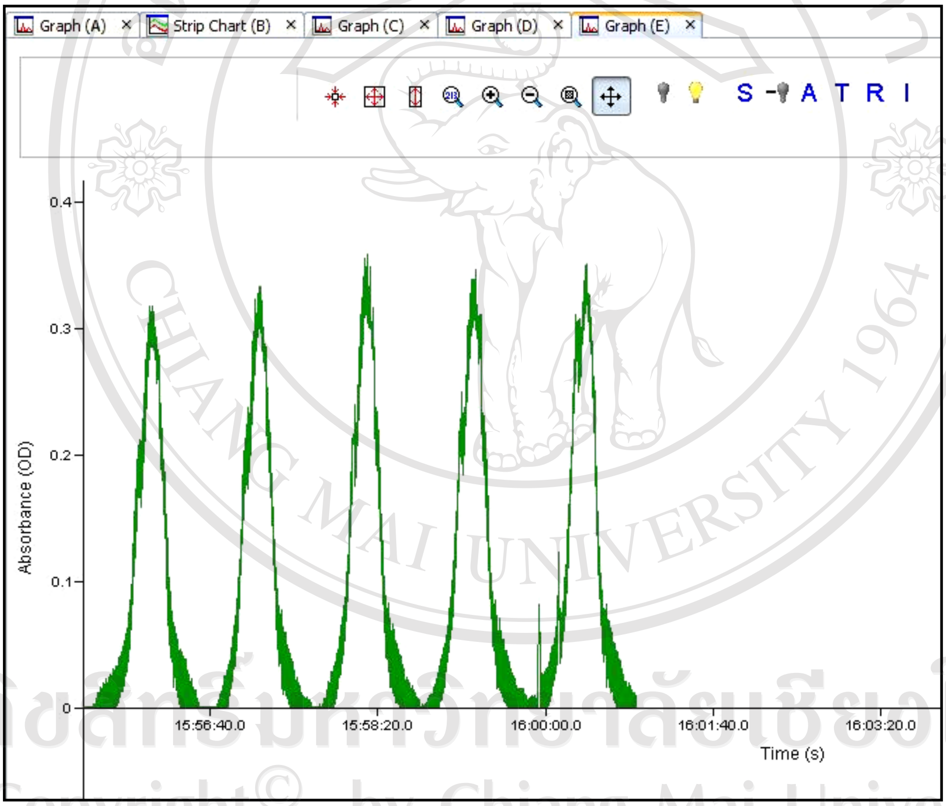

Figure 3.37 The absorption signal achieved from the Zn(II)-$(XO)_2$ complex (2.0 x 10^{-4} mol L^{-1} quinine hydrochloride, 1.5 mg L^{-1} Zn(II), pH 5, 2.0 x 10^{-4} mol L^{-1} XO) using the proposed method

ลิขสิทธิ์มหาวิทยาลัยเชียงใหม่
Copyright© by Chiang Mai University
All rights reserved

3.3.8.1 Optimum wavelength

The optimum wavelength for Zn(II) determination was examined over the range 575 – 600 nm by the proposed μFA system (Figure 3.35) using the experimental conditions as shown in Table 3.25. Therefore, it is essential to study the optimum wavelength of Zn(II)-$(XO)_2$. The results shown in Table 3.26 and Figure 3.38 indicated that the highest sensitivity was obtained when the absorbance was measured at 590 nm. The sensitivity was decreased above 590 nm. The optimum wavelength of 590 nm was selected for the further studies.

Table 3.26 Effect of wavelength on the sensitivity of Zn(II)-$(XO)_2$ complex

λ	**ΔP.H.* (AU) obtained from the standard Zn(II) (mg L^{-1})**					**y = mx + c**	**r^2**
	0.20	**0.30**	**0.40**	**0.50**	**0.60**		
575	0.055	0.072	0.091	0.108	0.125	0.1760x + 0.0198	0.9996
580	0.058	0.082	0.101	0.116	0.135	0.1880x + 0.0232	0.9936
585	0.063	0.087	0.107	0.128	0.145	0.2050x + 0.0240	0.9968
590	0.069	0.092	0.112	0.134	0.154	0.2118x + 0.0277	0.9995
595	0.066	0.092	0.108	0.129	0.148	0.2012x + 0.0281	0.9956
600	0.064	0.087	0.101	0.122	0.139	0.1850x + 0.0286	0.9957

*average of five replicate results

ลิขสิทธิ์มหาวิทยาลัยเชียงใหม่
Copyright© by Chiang Mai University
All rights reserved

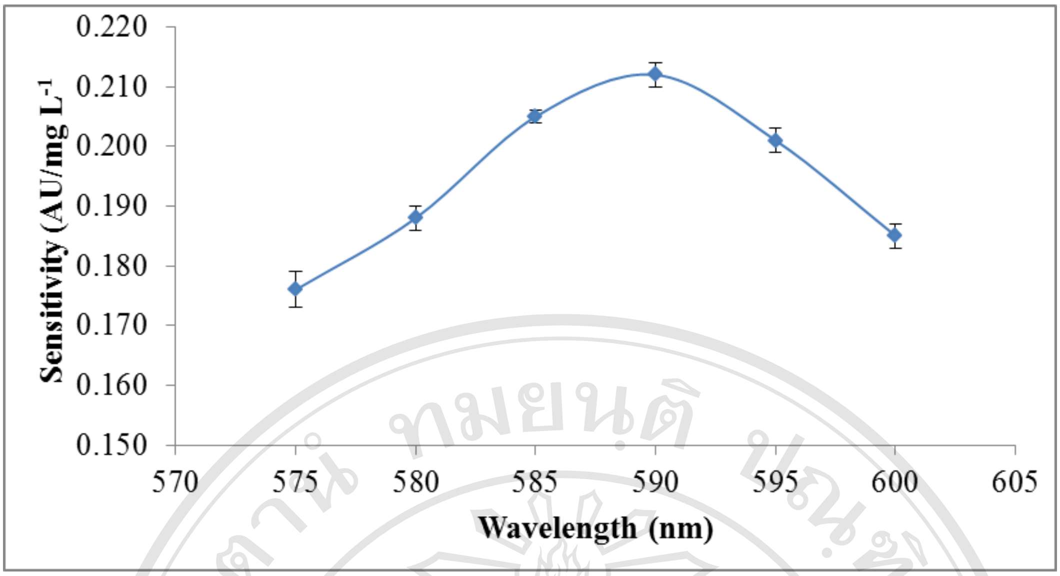

Figure 3.38 Effect of varying wavelength on the sensitivity for Zn determination

3.3.8.2 Effect of pH

As mentioned earlier (section 3.3.3), the pH of solution not only affect on the selectivity, however, it also influenced on the stoichiometry of the complexes resulting in hypsochromic shift and/or bathochromic shift of the maximum absorption wavelength (λ_{max}) depending on the reaction concerns. Therefore, it is essential to examine the effect of pH on the absorbance of the Zn(II)-$(XO)_2$ complex at 590 nm. This procedure was studied at various pH values in acetate buffer medium in the range of 4.0 to 6.5 using 1.0 x 10^{-4} mol L^{-1} quinine hydrochloride as photosensitizer. The results were shown in Table 3.27 and plotted in Figure 3.39. It was clear that when the pH of the acetate buffer stream was adjusted to 5.5, the greatest sensitivity was obtained. When the pH exceeded 5.5, the sensitivity significantly decreased until 6.5 because at pH lower than 5.5 the Zn(II)-$(XO)_2$ complex might not be formed effectively and at pH greater than 5.5 the complex might be suppressed from the residual red color XO resulting in low absorbance. Hence, pH 5.5 was selected throughout the next experiment.

ลิขสิทธิ์มหาวิทยาลัยเชียงใหม่
Copyright© by Chiang Mai University
All rights reserved

Table 3.27 The effect of pH on the sensitivity of Zn(II)-$(XO)_2$ complex measured at 590 nm

pH	ΔP.H.* (AU) obtained from the standard Zn(II) (mg L^{-1})					y = mx + c	r^2
	0.20	0.30	0.40	0.50	0.60		
4.0	0.069	0.092	0.112	0.134	0.154	0.2118x + 0.0277	0.9995
4.5	0.071	0.095	0.117	0.142	0.162	0.2290x + 0.0259	0.9985
5.0	0.075	0.106	0.125	0.147	0.176	0.2428x + 0.0288	0.9941
5.5	0.078	0.096	0.122	0.154	0.180	0.2630x + 0.0207	0.9924
6.0	0.067	0.086	0.113	0.144	0.157	0.2398x + 0.0173	0.9874
6.5	0.026	0.055	0.073	0.084	0.112	0.2002x - 0.0102	0.9788

*average of five replicate results

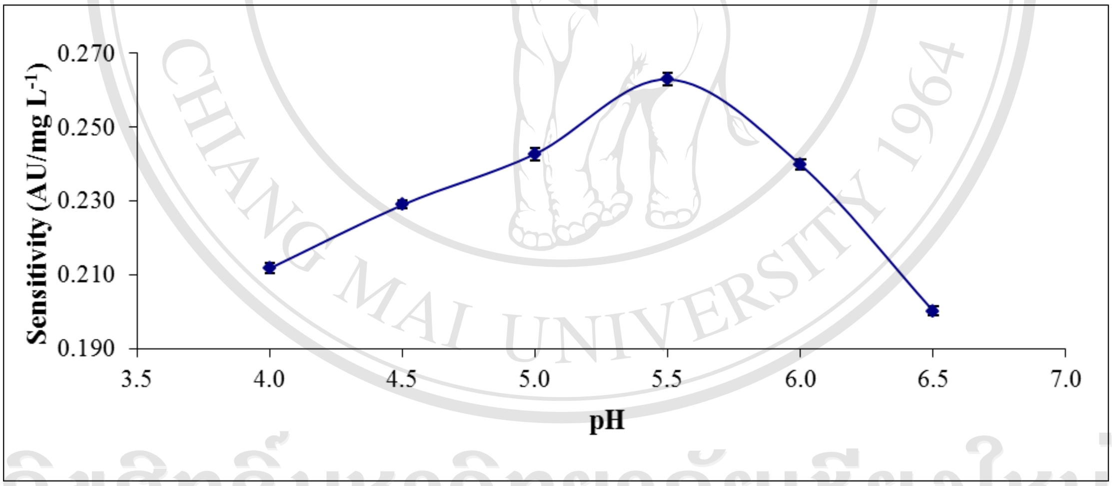

Figure 3.39 Effect of pH on the sensitivity of Zn(II)-$(XO)_2$ complex

ลิขสิทธิ์มหาวิทยาลัยเชียงใหม่
Copyright © by Chiang Mai University
All rights reserved

3.3.8.3 Effect of xylenol orange concentration

The concentration of reagent greater than that required by stoichiometry (Zn(II) : XO = 1:2) is demanded for completely color development. The effects of XO concentration was investigated over the range of 0.25 x 10^{-4} to 2.5 x 10^{-4} mol L^{-1} on the sensitivity of Zn(II)-$(XO)_2$ complex using 1.0 x 10^{-4} mol L^{-1} quinine hydrochloride as photosensitizer. The results were shown in Table 3.28 and Figure 3.40. It can be seen that the sensitivity of the complex increased with increasing XO concentration from 0.25 x 10^{-4} to 1.0 x 10^{-4} mol L^{-1}, above this the sensitivity slightly decreased owing to the concentration of XO lower than 1.0 x 10^{-4} mol L^{-1} is not sufficient to form complex with Zn(II) effectively. The concentration of XO beyond the upper limit caused suppression of color of Zn(II)-$(XO)_2$ complex absorbance resulting in low absorbance. Therefore, the optimum concentration of XO was 1.0 x 10^{-4} mol L^{-1}.

Table 3.28 Effect of several concentration of xylenol orange on the sensitivity

XO (x 10^{-4} mol L^{-1})	**ΔP.H.* (AU) obtained from the standard Zn(II) (mg L^{-1})**					**y = mx + c**	**r^2**
	0.20	**0.30**	**0.40**	**0.50**	**0.60**		
0.25	0.073	0.093	0.123	0.149	0.165	0.2402x + 0.0244	0.9918
0.50	0.077	0.096	0.123	0.154	0.182	0.2674x + 0.0195	0.9927
1.0	0.080	0.099	0.133	0.164	0.199	0.3034x + 0.0134	0.9917
1.5	0.075	0.094	0.122	0.158	0.189	0.2910x + 0.0112	0.9897
2.0	0.074	0.089	0.118	0.153	0.185	0.2862x + 0.0091	0.9835
2.5	0.064	0.084	0.107	0.144	0.176	0.2848x + 0.0011	0.9864

*average of five replicate results

ลิขสิทธิ์มหาวิทยาลัยเชียงใหม่
Copyright© by Chiang Mai University
All rights reserved

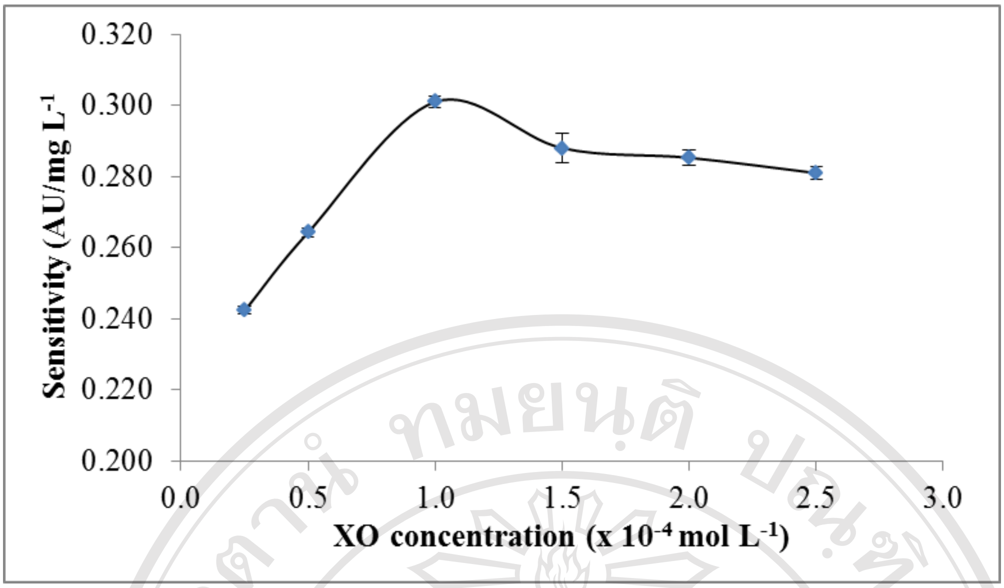

Figure 3.40 Effect of XO concentration on the sensitivity of Zn(II)-$(XO)_2$ complex

3.3.8.4 Effect of quinine hydrochloride concentration

The Effect of quinine concentration on the sensitivity of Zn(II)-$(XO)_2$ complex was studied at different values in the range of 0.05x 10^{-3} to 2.5 x 10^{-3} mol L^{-1}. The results are shown in Table 3.29 and Figure 3.41. It was found that sensitivity increased very rapidly from the quinine concentration of 0.05 x 10^{-4} – 1.0 x 10^{-3} mol L^{-1}. After that, the sensitivities were quite constant. Due to the fact that increasing the quinine hydrochloride concentration leading to the increase in the amounts of Zn(II)-$(XO)_2$ complexation which results in a higher sensitivity of the method achieved. However, outside the quinine hydrochloride concentration of 1.0 x 10^{-3} mol L^{-1}, the sensitivity of Zn(II)-$(XO)_2$ complexation became constant. Therefore, a concentration of 1.0×10^{-3} mol L^{-1} was chosen as the optimum photosensitizer concentration.

ลิขสิทธิ์มหาวิทยาลัยเชียงใหม่
Copyright© by Chiang Mai University
All rights reserved

Table 3.29 Effect of concentration of quinine hydrochloride on the sensitivity

Quinine hydrochloride concentration ($\times 10^{-3}$ mol L^{-1})	**ΔP.H.* (AU) obtained from the standard Zn(II) (mg L^{-1})**					**y = mx + c**	**r^2**
	0.20	**0.30**	**0.40**	**0.50**	**0.60**		
0.05	0.068	0.096	0.126	0.154	0.182	0.2868x + 0.0105	0.9997
0.10	0.079	0.099	0.133	0.163	0.198	0.3032x + 0.0132	0.9930
0.50	0.079	0.104	0.138	0.173	0.215	0.3416x + 0.0051	0.9931
1.0	0.078	0.107	0.142	0.178	0.223	0.3622x + 0.0006	0.9938
2.0	0.077	0.106	0.141	0.176	0.220	0.3568x + 0.0013	0.9948
2.5	0.078	0.107	0.143	0.177	0.222	0.3588x + 0.0020	0.9941

*average of five replicate results

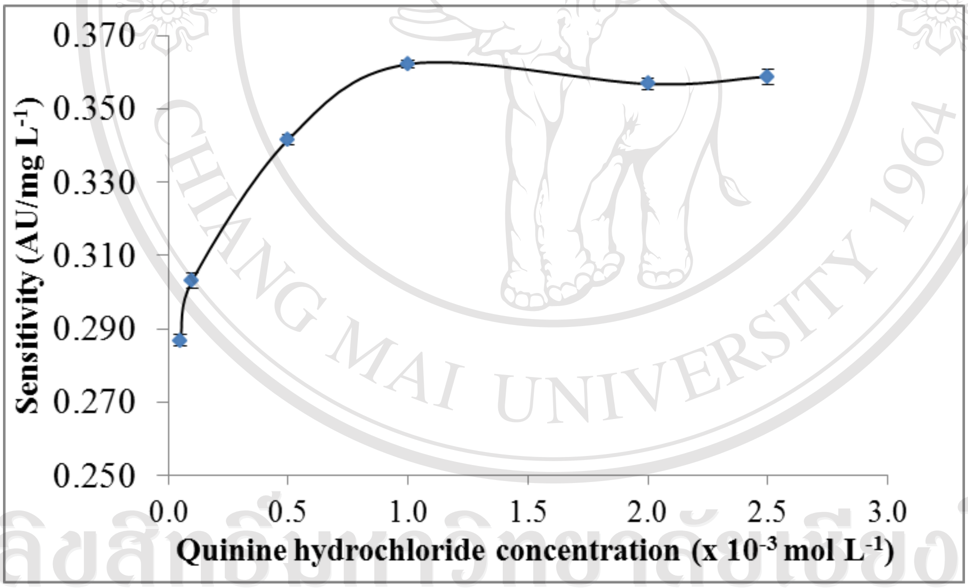

Figure 3.41 Effect of quinine hydrochloride on the sensitivity of Zn(II)-$(XO)_2$ complex

ลิขสิทธิ์มหาวิทยาลัยเชียงใหม่
Copyright© by Chiang Mai University
All rights reserved

3.3.8.5 The effect of flow rate

The effect of flow rate on the sensitivity of Zn(II)-$(XO)_2$ complex was studied for Zn(II) determination. A high flow rate leads to a shorter time for each sample passing through the detection cell resulting in a little amount of products, poor reproducibility and high reagent consumption. The low flow rate of solution, the residence time for each standard/sample is long and the dispersion zone is large size that can reduce the sensitivity and the sample throughput. The total flow rate was varied over the range of 20 - 70 μL min^{-1}. The effect of flow rate on the sensitivity was shown in Table 3.30. Figure 3.42 displayed that the sensitivity of Zn(II)-$(XO)_2$ complex increases with increasing flow rate to 40 μL min^{-1} due to low flow rate expanded dispersion zone. After that, the sensitivity was reduced when the flow rate was higher than 40 μL min^{-1} due to the fact that the upper flow rate reduced the reaction time and the number of complex formation. Therefore, the optimum flow rate for delivering xylenol orange reagent was 40 μL min^{-1}.

Table 3.30 Effect of flow rate on the sensitivity of Zn(II)-$(XO)_2$

Flow rate (μL min^{-1})	**ΔP.H.* (AU) obtained from the standard Zn(II) (mg L^{-1})**					**y = mx + c**	**r^2**
	0.20	**0.30**	**0.40**	**0.50**	**0.60**		
20	0.059	0.0960	0.125	0.165	0.184	y = 0.3202x - 0.0024	0.9907
30	0.067	0.097	0.132	0.173	0.205	y = 0.3522x - 0.0062	0.9976
40	0.078	0.107	0.141	0.177	0.223	y = 0.3612x + 0.0008	0.9927
50	0.066	0.096	0.135	0.172	0.204	y = 0.3524x - 0.0061	0.9983
60	0.047	0.086	0.115	0.145	0.163	y = 0.2926x - 0.0059	0.9858
70	0.038	0.064	0.084	0.122	0.145	Y = 0.2734x - 0.0188	0.9907

*average of five replicate results

ลิขสิทธิ์มหาวิทยาลัยเชียงใหม่
Copyright © by Chiang Mai University
All rights reserved

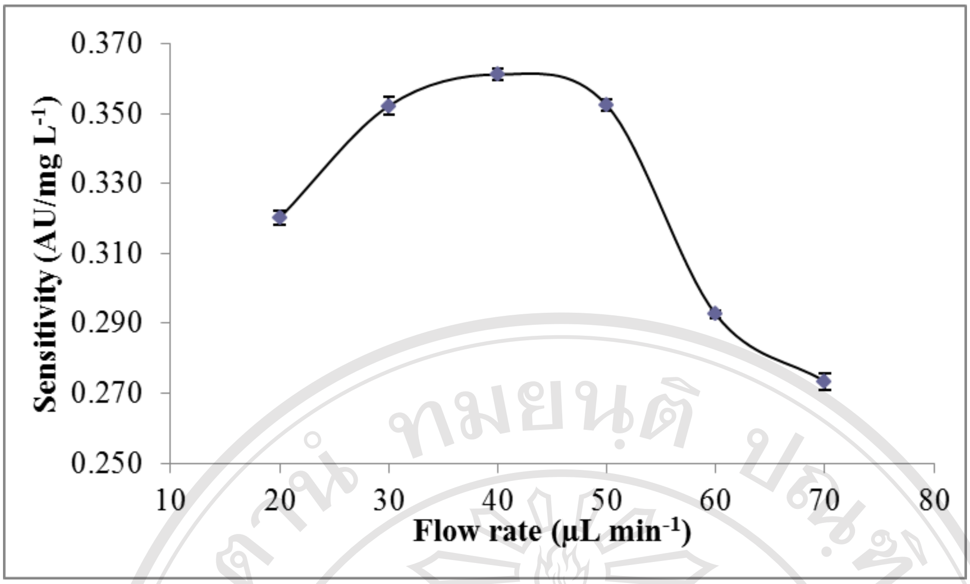

Figure 3.42 Effect of flow rate on the sensitivity of Zn(II)-$(XO)_2$ complex

3.3.8.6 Effect of sample introduction volume

The sample volume injection into the xylenol orange stream has an important effect on sensitivity. The influence of sample injection volume on the sensitivity of Zn(II)-$(XO)_2$ complex was examined by controlling pump flow rate and the switching time of the selection valve at sample line over the range of 2.0 - 7.0 µL of standard Zn(II). The results were displayed in Table 3.31 and Figure 3.43. It was seen that initially the sensitivity increased rapidly with increasing sample volume up to 5.0 µL due to increasing sample volume leading to raise the increment of quantity of the complex. After that, the sensitivity increased slightly and peak broadening was also observed leading to the larger dispersion zone was achieved as soon as the sample volume was increased to some extents (6 µL). Therefore, the injection volume of 5.0 µL was selected to be the optimum value because of a reasonable compromise between good sensitivity and reagent consumption.

ลิขสิทธิ์มหาวิทยาลัยเชียงใหม่
Copyright© by Chiang Mai University
All rights reserved

Table 3.31 Effect of injection volume on the sensitivity of Zn(II)-$(XO)_2$

Sample volume (μL)	**ΔP.H.* (AU) obtained from the standard Zn(II) (mg L^{-1})**					**y = mx + c**	**r^2**
	0.20	**0.30**	**0.40**	**0.50**	**0.60**		
2.0	0.057	0.081	0.102	0.123	0.133	y = 0.1926x + 0.0222	0.9819
3.0	0.061	0.081	0.114	0.137	0.162	y = 0.2564x + 0.0084	0.9957
4.0	0.071	0.091	0.131	0.169	0.212	y = 0.3584x - 0.0086	0.9871
5.0	0.078	0.107	0.145	0.182	0.225	y = 0.3690x - 0.0003	0.9957
6.0	0.072	0.105	0.146	0.184	0.224	y = 0.3834x - 0.0072	0.9988
7.0	0.067	0.105	0.141	0.184	0.225	Y = 0.3954x - 0.0138	0.9989

*average of five replicate results

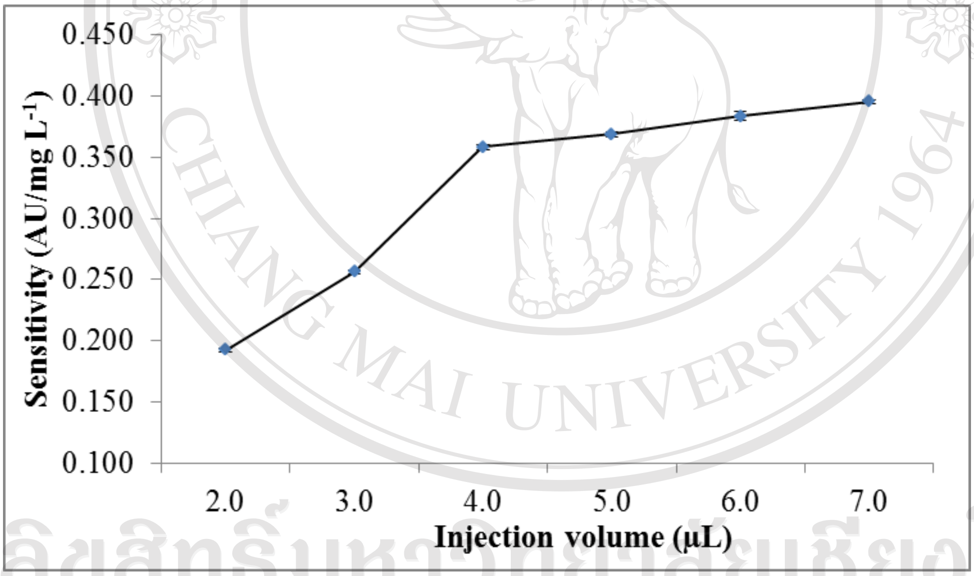

Figure 3.43 Effect of sample introduction volume on the sensitivity of Zn(II)-$(XO)_2$ complex

ลิขสิทธิ์มหาวิทยาลัยเชียงใหม่
Copyright© by Chiang Mai University
All rights reserved

The optimum values of all the experimental parameters were studied by using the proposed μFA system integrated with the PMMA chip, the optimized conditions for determination of Zn(II) based on reaction with XO in the presence of quinine hydrochloride as photosensitizer were displayed in Table 3.32.

Table 3.32 Optimum conditions for Zn(II) determination using the home-made PMMA microflow analyzer

Parameters	Range studied	Optimum value
Wave length (nm)	575-600	590
pH	4.0-6.5	5.5
XO concentration (x 10^{-4} mol L^{-1})	0.25-2.5	1.0
Quinine hydrochloride concentration (x 10^{-3} mol L^{-1})	0.05-2.5	1.0
Injection volume (μL)	2-7	5.0
Flow rate (μL min^{-1})	20-70	40.0
Reaction channel (width x depth x Length)	-	194 μm x 195 μm x 200 mm

3.3.9 Analytical characteristics

3.3.9.1 Linear range

The linear range of the proposed method was investigated by flowing Zn(II) standard solution into μFA system under the optimum conditions that were presented previously. Linear range of the calibration graph was studied for Zn(II) standards at the concentration ranging from 0.01–1.8 mg L^{-1}. All measurements were made in five replication injections. The results obtained are displayed in Table 3.33 and Figure 3.4.

ลิขสิทธิ์มหาวิทยาลัยเชียงใหม่
Copyright© by Chiang Mai University
All rights reserved

Table 3.33 Linearity of Zn(II) determination with µFA system

Zinc (mg L^{-1})	Peak height (AU)							ΔP.H. (AU)
	1	2	3	4	5	$\bar{x}$	SD	
0.00	0.009	0.008	0.01	0.011	0.009	0.009	-	-
0.01	0.017	0.019	0.018	0.016	0.018	0.018	0.001	0.009
0.05	0.025	0.026	0.026	0.027	0.027	0.026	0.001	0.017
0.10	0.054	0.055	0.053	0.054	0.055	0.054	0.001	0.045
0.20	0.085	0.086	0.087	0.088	0.089	0.087	0.001	0.078
0.30	0.118	0.117	0.117	0.118	0.119	0.118	0.002	0.109
0.40	0.146	0.151	0.150	0.153	0.151	0.151	0.001	0.142
0.50	0.188	0.187	0.189	0.188	0.189	0.188	0.003	0.179
0.60	0.225	0.229	0.235	0.226	0.229	0.229	0.001	0.220
0.70	0.265	0.267	0.266	0.265	0.266	0.266	0.004	0.257
0.80	0.298	0.297	0.297	0.301	0.302	0.299	0.001	0.290
0.90	0.332	0.331	0.331	0.331	0.333	0.332	0.002	0.323
1.00	0.369	0.364	0.365	0.366	0.365	0.366	0.001	0.357
1.10	0.393	0.394	0.389	0.395	0.392	0.393	0.002	0.384
1.20	0.422	0.423	0.424	0.422	0.423	0.423	0.002	0.414
1.30	0.452	0.453	0.454	0.455	0.454	0.454	0.001	0.445
1.40	0.485	0.486	0.485	0.486	0.485	0.485	0.001	0.476
1.50	0.522	0.523	0.524	0.521	0.519	0.522	0.001	0.513
1.60	0.528	0.522	0.521	0.524	0.524	0.524	0.002	0.515
1.70	0.525	0.538	0.537	0.536	0.546	0.536	0.003	0.527
1.80	0.540	0.541	0.538	0.541	0.538	0.540	0.008	0.531

ลิขสิทธิ์มหาวิทยาลัยเชียงใหม่
Copyright© by Chiang Mai University
All rights reserved

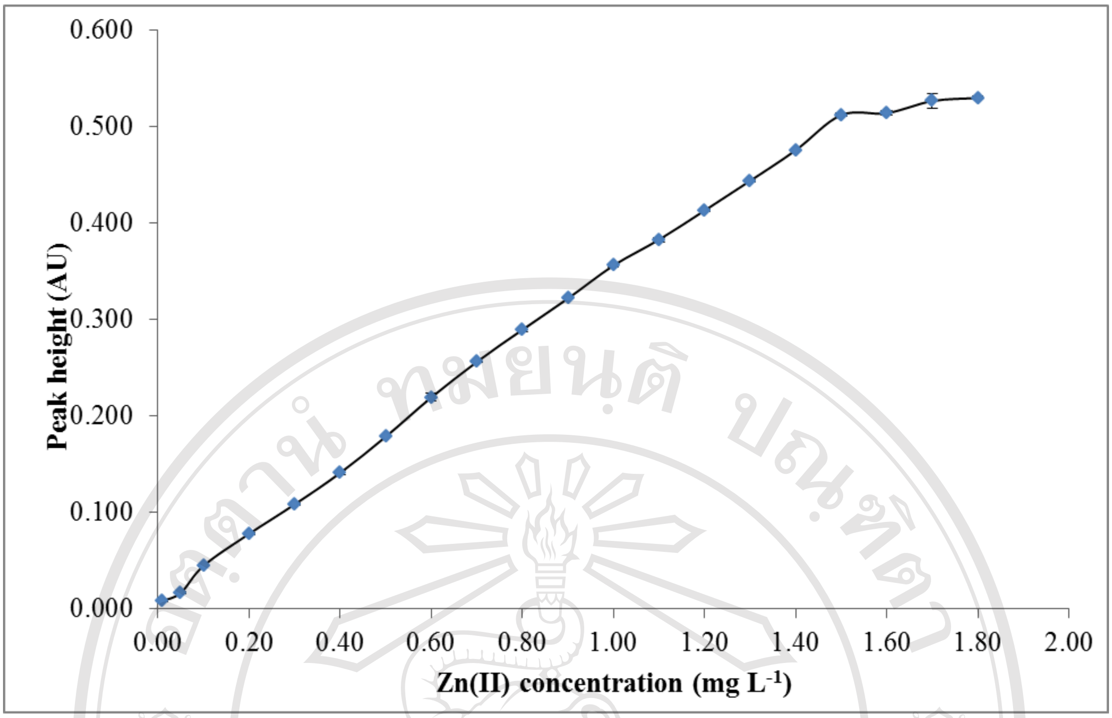

Figure 3.44 Relationship between peak height and concentrations of Zn(II) 0.01-1.8 mg L^{-1}

3.3.9.2 Precision and accuracy of the proposed method

The precision of the proposed system based on repeatability was accomplished by 11-replicates of two standard solutions covering different concentrations as 0.5 and 1.0 mg L^{-1} and the peak heights of which as absorbance were measured, the results were displayed in Table 3.34. Statistical evaluation revealed that the relative standard deviations (RSD) of the two concentrations of Zn(II) standard solutions were found to be 1.20 and 1.12%, respectively. In addition, the accuracy of the proposed method was examined, the percentage recoveries were investigated by spiking 0.5 μg mL^{-1} Zn(II) standard solutions into water samples. The results indicated that the percentage recoveries of Zn(II) added were in the range of 98.21 - 102.8 % (Table 3.38). Moreover, the developed method was rapid with an average t_{base} of 90 s (n=7)

ลิขสิทธิ์มหาวิทยาลัยเชียงใหม่
Copyright© by Chiang Mai University
All rights reserved

together with the sample throughput for the proposed method was found to be 40 samples h^{-1}.

Table 3.34 The precision study using two standard solutions (0.5 and 1.0 mg mL^{-1})

Experiment number	Absorbance (AU)	
	Concentration of standard Zn(II) (mg L^{-1})	
	0.5	**1.0**
1	0.179	0.361
2	0.178	0.36
3	0.182	0.357
4	0.181	0.358
5	0.183	0.353
6	0.176	0.357
7	0.177	0.352
8	0.179	0.362
9	0.181	0.356
10	0.181	0.354
11	0.179	0.365
$\bar{x}$	0.180	0.358
SD	2.16E-03	4.00E-03
%RSD	1.20	1.12

3.3.9.3 Calibration curve

Calibration curve was obtained by measurement of the absorbance of the complex using Zn(II) standard solutions over the range of 0.1 to 1.5 mg L^{-1} under the optimum conditions as shown in Table 3.32. All measurements were made in five replicate injections, the μFA-grams was displayed in Figure 3.45. The results were summarized in Table 3.35 and Figure 3.46. It was found that the calibration graph was expressed by the regression equation y = 0.3481x + 0.007 (n=5) (r^2 = 0.9996), where y is absorbance of Zn(II)-$(XO)_2$ complex and x is Zn(II) concentrations (mg L^{-1}).

ลิขสิทธิ์มหาวิทยาลัยเชียงใหม่
Copyright © by Chiang Mai University
All rights reserved

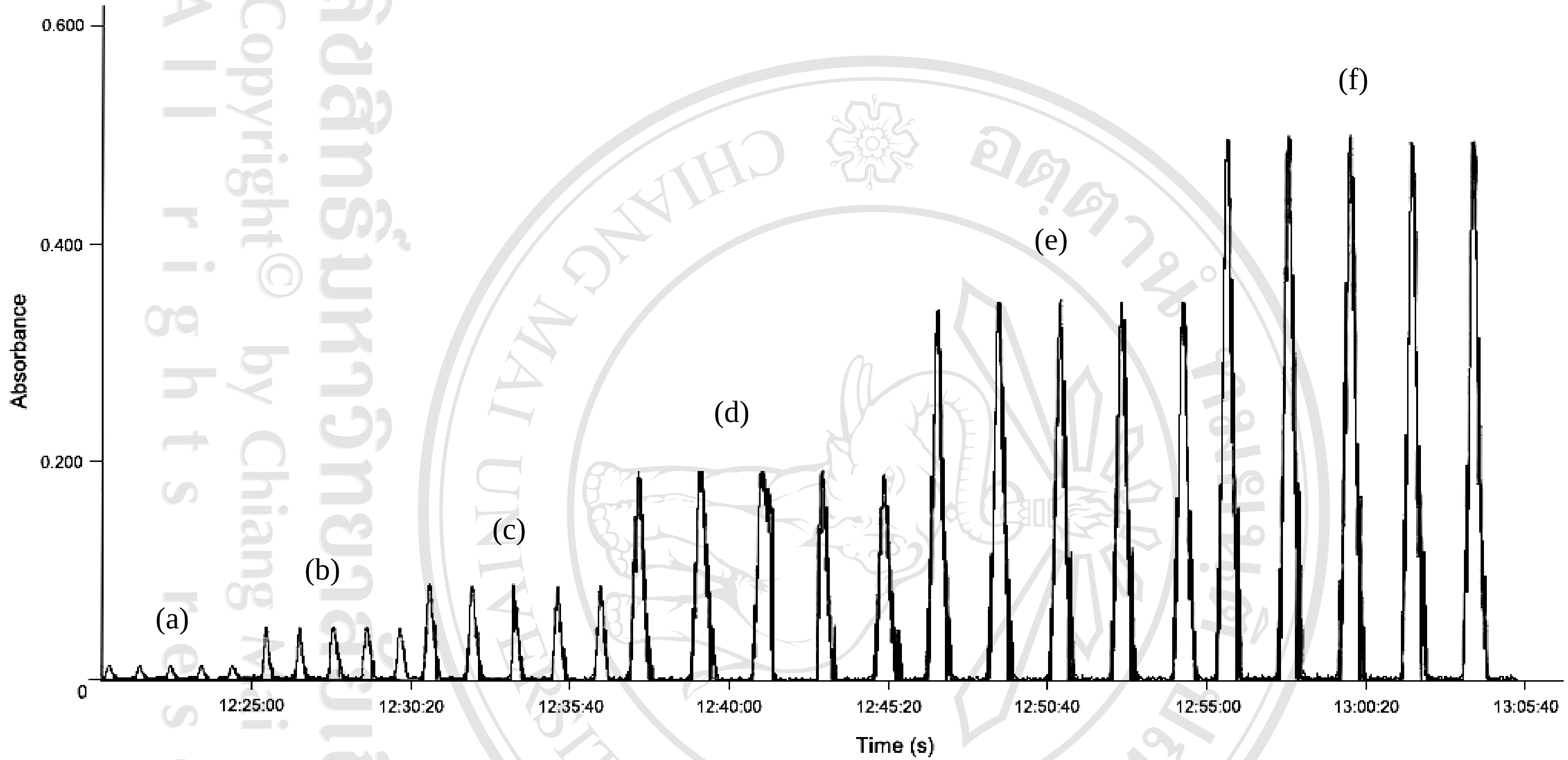

Figure 3.45 μFA grams for determining Zn(II) as Zn(II)-$(XO)_2$ using the proposed μFA under the optimum conditions, Zn(II) concentrations; (a) blank, (b) 0.1 mg L^{-1}, (c) 0.2 mg L^{-1}, (d) 0.5 mg L^{-1} , (e) 1.0 mg L^{-1} and (f) 1.5 mg L^{-1}

ลิขสิทธิ์มหาวิทยาลัยเชียงใหม่
Copyright© by Chiang Mai University
All rights reserved

Table 3.35 The absorbance of Zn(II)-$(XO)_2$ complex for calibration curve

Zn(II) (μg mL^{-1})	**Peak height (AU)***						
	1	**2**	**3**	**4**	**5**	$\bar{x}$	**SD**
0.10	0.044	0.042	0.042	0.041	0.042	0.042	0.0011
0.20	0.078	0.08	0.078	0.081	0.077	0.079	0.0016
0.50	0.179	0.181	0.180	0.178	0.177	0.179	0.0016
1.0	0.362	0.354	0.358	0.355	0.362	0.358	0.0038
1.5	0.527	0.525	0.526	0.527	0.526	0.526	0.0008

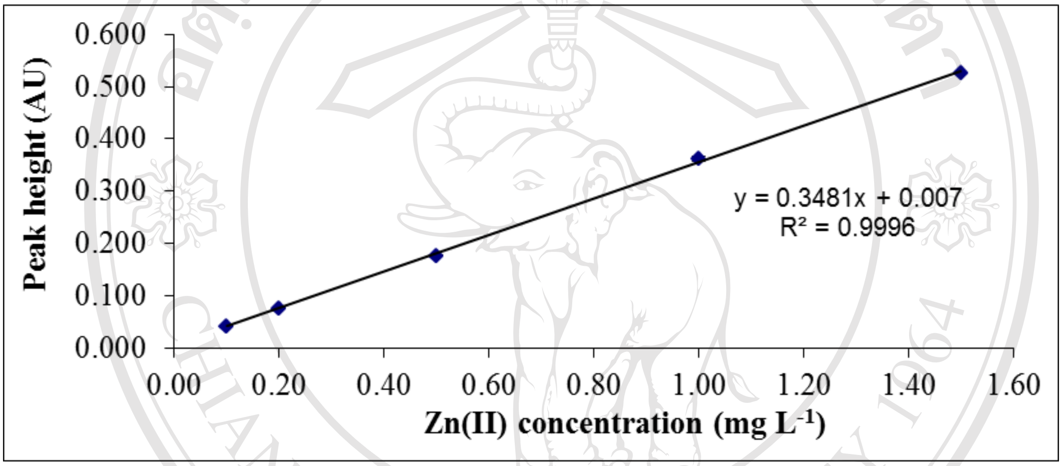

Figure 3.46 Calibration curve of the μFA system for zinc determination

3.3.9.4 Detection limit [259]

Detection limit was calculated from the linear regression line of calibration curve of analyte with the considered parameters of the intercept of the straight line and three-times the standard deviation of the regression time and with the limit of quantitation (ten-times the standard deviation of the regression time). The results are giving in Tables 3.36. The concentration at limit of detection (LOD) can be calculated from equation 2.3-2.4. It was found that the LOD of the proposed μFA was 0.06 mg L^{-1} and LOQ was 0.19 mg L^{-1}.

ลิขสิทธิ์มหาวิทยาลัยเชียงใหม่
Copyright© by Chiang Mai University
All rights reserved

Table 3.36 Calculation of detection limit of μFA spectrophotometric determination of zinc (II)

Zn (mgL-1)	Y_i^*	$\hat{Y}_i$	$\lvert Y_i^* - \hat{Y}_i \rvert$	$\lvert Y_i^* - \hat{Y}_i \rvert^2$
0.10	0.042	0.0418	0.0004	1.52E-07
0.20	0.079	0.0766	0.0022	4.75E-06
0.50	0.179	0.1811	0.0021	4.2E-06
1.0	0.358	0.3551	0.0029	8.41E-06
1.5	0.519	0.5292	0.0106	0.000111
$\sum(\lvert Y_i^* - \hat{Y}_i \rvert^2)$				0.000129
S_y/x				0.006553
C_L,LOD				0.056
LOQ				0.188

The linear regression equation is Y = 0.3481 + 0.007

$$Sy/x = [0.000129/(5-2)]^{1/2}$$

$$= 0.006553$$

$$C_L\text{, LOD} = (3 \times 0.006553)/0.3481$$

$$= 0.056 \text{ mg L}^{-1} \text{ Zn(II)}$$

$$\text{LOQ} = (10 \times 0.006553)/0.3481$$

$$= 0.188 \text{ mg L}^{-1} \text{ Zn(II)}$$

ลิขสิทธิ์มหาวิทยาลัยเชียงใหม่
Copyright© by Chiang Mai University
All rights reserved

3.3.9.5 Interference studies

Investigation of the selectivity of the proposed method, the effect of some possible interferences ions which are present together with zinc(II) in water samples, were investigated using 0.5 mg L^{-1} of Zn(II). The effect of common ions in the determination of 0.5 mg L^{-1} Zn(II) was studied. The tolerance limit of interfering ion was taken as the maximum amount (mg L^{-1}) causing an error not greater than ±10% for determining the target analyte [263]. The tolerance concentrations of the studied species to 0.5 mg L^{-1} Zn(II) under the optimum conditions as summarized in Table 3.37. Most ions studied did not interfere for the determination of Zn(II) except Cu(II), Fe(III) and Al(III). Especially, Fe(III) is present in the water samples in several mg L^{-1}. Therefore, these ions must be eliminated prior determination of Zn(II). Fe(III) and Al(III) can be removed prior to analysis of Zn(II) by using 0.20% w/v sodium fluoride as masking agent. Cu(II) can be eliminated by using 0.05% sodium thiosulfate pentahydrate and the careful control of the pH of the acetate buffer solution. However, the absorbance of Zn(II)-$(XO)_2$ is reduced if adding a lot of sodium thiosulfate pentahydrate that is block the reaction between Zn(II) and XO . Moreover, Ni(II) is present in natural water samples in trace levels, therefore, Ni(II) can be considered to be no interference in case of Zn(II) determination in natural water. The studied marking agents were displayed in Table 2E (appendix E).

ลิขสิทธิ์มหาวิทยาลัยเชียงใหม่
Copyright© by Chiang Mai University
All rights reserved

Table 3.37 Tolerable levels of interfering ions effect on the absorption signal

Interference ions	**Tolerable concentration ratio[a] (mg L^{-1}) of ion/Zn(II) 0.5 mg L^{-1}**
Mg^{2+}, Cd^{2+}, Mn^{2+}, SO_4^{2-}, PO_4^{3-}, Cl^-, Br^-, I^-, NO_3^-, Na^+, K^+	≥1000
Ca^{2+},Cr^{3+}, Co^{2+}	700
NO_2^-, Ba^{2+},	500
HCO_3^-	100
Ni^{2+}, Pb^{2+}	20
Al^{3+}	20 ([b])
Fe^{3+}	20 ([b])
Cu^{2+}	20 ([c])

[a] The foreign species concentration causing error smaller than ±10% for request to the signal Zn(II) alone

[b] 0.20% Sodium fluoride as masking agent

[c] 0.05% Sodium thiosulfate pentahydrate

3.3.10 Determination of Zn(II) in water samples

The proposed μFA system integrated with the PMMA chip was applied to the determination of ZnII) in natural water samples which were collected from Kuang river in Lam Phun Province, Thailand where the Northern Industrial Estate is located (W1 to W7). The results are given in Table 3.38 compared with those obtained by FAAS. It is displayed that the results obtained by the proposed PMMA chip agree well with those obtained by FAAS, because the calculated student t-value (appendix C) was less than the theoretical value (4.30) at confident level of 95% (Table 3.39). The amounts of Zn(II) in water samples analyzed by the proposed system were in the range of 0.160-0.474 mg L^{-1}. With respect to the amounts of chemical and reagents

ลิขสิทธิ์มหาวิทยาลัยเชียงใหม่
Copyright© by Chiang Mai University
All rights reserved

consumption, the proposed micro flow analysis method consumed smaller amount of chemical and reagent than those consumed by other methods; it also released smaller waste than those produced by other methods such as conventional FIA. Since the proposed microflow analyzer was miniaturized components (selection valve, peristaltic pump and fiber optic spectrometer) and a laptop for data manager that seem promising for adoption to being portable and suitable for on site monitoring.

Table 3.38 Concentrations of Zn(II) in water sample (mg L^{-1}) analyzed by using the proposed μFA

Water samples	**Zn(II) found (mg L^{-1})**				**S.D.**	**Zn(II) concentration* (mg L^{-1})**	**% Recovery**
	1	**2**	**3**	**$\bar{x}$**			
W1	0.212	0.225	0.226	0.221	0.0078	0.221 ± 0.008	98.5
W2	0.157	0.161	0.162	0.160	0.0026	0.160 ± 0.003	101.5
W3	0.342	0.345	0.347	0.345	0.0025	0.345 ± 0.003	98.3
W4	0.453	0.455	0.457	0.455	0.0020	0.455 ± 0.002	98.2
W5	0.475	0.474	0.472	0.474	0.0015	0.474 ± 0.002	98.4
W6	0.182	0.178	0.195	0.185	0.0089	0.185 ± 0.009	102.8
W7	ND**	ND**	ND**	-	-	ND**	102.5

*average of triplicate results

**not detected

ลิขสิทธิ์มหาวิทยาลัยเชียงใหม่
Copyright© by Chiang Mai University
All rights reserved

Table 3.39 Comparative determination of Zn(II) in water samples by proposed PMMA chip and FAAS

Water sample	**Concentrations (mg L^{-1})**		$t_{\text{calculated}}$
	μFA*	**FAAS***	
W1	0.221	0.233	-2.661
W2	0.160	0.165	-3.273
W3	0.345	0.341	2.524
W4	0.455	0.451	3.464
W5	0.474	0.471	3.024
W6	0.185	0.171	2.728
W7	ND**	ND**	-

*average of triplicate results

**not detected

ลิขสิทธิ์มหาวิทยาลัยเชียงใหม่
Copyright© by Chiang Mai University
All rights reserved